B. Siemon, W. Voß, M. Ibs-von Seht,
A. Ullmann, J. Pielawa

Bundesanstalt für
Geowissenschaften
und Rohstoffe

Airborne Geophysical Investigations of CLIWAT Pilot Areas

Survey Area Vojens, Denmark, 2009

CLIWAT
CLIMATE & WATER

Interreg IVB Project:
CLIWAT – Adaptive and sustainable water management and protection of society and nature in an extreme climate

Bundesanstalt für Geowissenschaften und Rohstoffe
Federal Institute for Geosciences and Natural Resources

CLIWAT – Adaptive and sustainable water management and protection of society and nature in an extreme climate

Survey Area Vojens, Denmark

2009

Technical Report on the Interreg IVB Project

The project is part-financed by the European Union

In Cooperation with
Region Syddanmark
Vejle, Denmark

Authors: B. Siemon
W. Voß
M. Ibs-vonSeht
A. Ullmann
J. Pielawa

Date: September 15, 2010

Table of contents

Personnel III

List of figures IV

List of tables V

List of maps VI

List of vertical resistivity sections VII

Abbreviations VIII

1. Summary 1

2. Introduction 3

3. Survey Area 6

4. Airborne Geophysical System 8

4.1. The Helicopter 9

4.2. Measuring System 9

4.3. Electromagnetics 10

4.4. Magnetics 11

4.5. Radiometrics 12

4.6. Navigation and Positioning 13

4.7. Data Acquisition and Recording 15

4.8. Video System 15

4.9. Additional Equipment 16

5. Processing and Presentation of the Survey Data 17

5.1. General Processing Steps 17

5.2. Position Data 18

5.2.1. Coordinates 18
5.2.2. Radar Altitude 18
5.2.3. Laser Altitude 18
5.2.4. Topographic Elevation 19

5.3. Processing of the Electromagnetic Data 20

5.3.1. Calibration of the HEM System 20
5.3.2. Zero-Level and Drift Correction 21
5.3.3. Data Correction 21
5.3.4. Conversion of the Secondary Field Values to Half-Space Parameters 22
5.3.5. Effect of Anthropogenic Influences on the HEM Data 24

5.3.6. Statistical Levelling 25
5.3.7. 1-D Inversion of the HEM Data 26
5.3.8. Presentation of the Results 27

5.4. Processing of Magnetic Data 28

5.4.1. Magnetic Total Field 28
5.4.2. IGRF 28
5.4.3. Diurnal Variations 28
5.4.4. Levelling 28
5.4.5. Presentation of the Results 29

5.5. Processing of Gamma-Ray Spectrometry Data 30

5.5.1. Energy Calibration 30
5.5.2. Reduction of Statistical Noise 31
5.5.3. Detector Height above Ground and Effective Height 31
5.5.4. Live Time Correction 32
5.5.5. Background Radiation Correction 32
5.5.6. Compton Correction 33
5.5.7. Height-Attenuation Reduction 33
5.5.8. Radioelement Concentrations and Exposure Rate 34
5.5.9. Data Levelling and Smoothing 36
5.5.10. Presentation of the Results 36

6. Cartographic Work 37

6.1. Topographic Map 37

6.2. Map Production with GEOSOFT and GIS Software 37

6.3. Thematic Maps 38

7. Archiving 39

8. References 40

Signatures 41

Appendix I: Survey Area Vojens 42

Appendix II: Final Data Format Description 45

Appendix III: DVD 54

Appendix IV: Maps 57

Appendix V: Vertical Resistivity Sections 89

Personnel

Field Crew

Dr. Bernhard **Siemon**, project leader, field data processing, B2.1, BGR
Wolfgang **Voß**, navigation, B2.1, BGR
Karl-Heinz **Meinhardt**, system operation and engineering, B2.1, BGR
Josef **Scheiwein**, helicopter engineering, B2.1, BGR
Michael **Schütt**, pilot, Wiking Helikopter Service GmbH

Office Crew

Dr. Uwe **Meyer**, leader of sub-department B2.1, BGR
Dr. Bernhard **Siemon**, project leader, electromagnetic data evaluation, B2.1, BGR
Angelika **Ullmann**, project scientist, electromagnetic data evaluation, B2.1, BGR
Dr. Malte **Ibs-von Seht**, magnetic and radiometric data evaluation, B2.1, BGR
Jens **Pielawa**, cartographic work, B2.1, BGR

Address: Federal Institute for Geosciences and Natural Resources (BGR)
Stilleweg 2
30655 Hanover
Germany
Tel.: +49 511 643 3212 (Meyer)
3488 (Siemon)
Fax: +49 511 643 3663
Email: Uwe.Meyer@bgr.de, Bernhard.Siemon@bgr.de

List of figures:

1. Regions funded by the Interreg IVB North Sea Region Programme

2. Vojens survey area

3. Principal sketch of the BGR airborne geophysical system

4. HEM inversion based on a homogeneous half-space or a layered half-space

5. Construction of starting models

List of tables:

1. Survey parameters for the Vojens survey area

2. Technical specifications of the BGR helicopter D–HBGR

3. The geophysical survey systems

4. HEM system parameters (Bird 61)

5. Base stations

6. Radiation sources and corresponding spectrometer parameters

7. Navigation and positioning systems

8. Altimeters

9. Data acquisition and recording systems

10. Video system

11. Additional equipment

12. Filter parameters for the removal of the tree-canopy effect

13. Calibration factors of the HEM systems

14. Filter parameters for HEM data processing

15. Filter parameters for semi-automatic correction of man-made effects

16. Filter parameters for micro-levelling of log ρ_a and d_a

17. Filter parameters for the levelling of HEM data

18. Aircraft background and cosmic stripping factors

19. Stripping ratios

20. Height attenuation coefficient

21. Sensitivity coefficients

22. Linear attenuation coefficients μ for vegetation

23. Coordinates of the corners of the 1:25,000 Vojens topographic map sheet

24. Grid parameters

25. Content of the DVD

A-1 Flight table

List of maps:

1. Flight lines,
2. Digital elevation model,
3. Apparent resistivity at 133,200 Hz (rhoa6),
4. Apparent resistivity at 41,430 Hz (rhoa5),
5. Apparent resistivity at 8,389 Hz (rhoa4),
6. Apparent resistivity at 5,403 Hz (rhoa3),
7. Apparent resistivity at 1,820 Hz (rhoa2),
8. Apparent resistivity at 387 Hz (rhoa1),
9. Centroid depth at 133,200 Hz (zst6),
10. Centroid depth at 41,430 Hz (zst5),
11. Centroid depth at 8,389 Hz (zst4),
12. Centroid depth at 1,820 Hz (zst3),
13. Centroid depth at 1,820 Hz (zst2),
14. Centroid depth at 387 Hz (zst1),
15. Resistivity at 01 m bgl,
16. Resistivity at 03 m bgl,
17. Resistivity at 05 m bgl,
18. Resistivity at 10 m bgl,
19. Resistivity at 20 m bgl,
20. Resistivity at 30 m bgl,
21. Resistivity at 50 m bgl,
22. Resistivity at 70 m bgl,
23. Resistivity at 90 m bgl,
24. Resistivity at 120 m bgl,
25. Anomalies of the total magnetic field (ΔT),
26. Anomalies of the total magnetic field (ΔT), high-pass filtered, anthropogenic anomalies removed,
27. Concentration of Potassium (K),
28. Concentration of Thorium (Th),
29. Concentration of Uranium (U),
30. Stripped total count rate (TC),
31. Ground level exposure rate in μR/h.

List of vertical resistivity sections:

Tie lines:

1. VRS 1.9,
2. VRS 2.9,
3. VRS 3.9,
4. VRS 4.9,
5. VRS 5.9,
6. VRS 6.9,
7. VRS 7.9,
8. VRS 8.9,
9. VRS 9.9,
10. VRS 10.8,
11. VRS 11.9,
12. VRS 12.9,
13. VRS 13.9,
14. VRS 14.9,
15. VRS 15.9,
16. VRS 16.9,

Lines:

17. VRS 1.1,
18. VRS 2.1,
19. VRS 3.1,
20. VRS 4.1,
21. VRS 5.1,
22. VRS 6.1,
23. VRS 7.1,
24. VRS 8.1,
25. VRS 9.1,
26. VRS 10.1,
27. VRS 11.1,
28. VRS 12.1,
29. VRS 13.1,
30. VRS 14.1,
31. VRS 15.1,
32. VRS 16.1,
33. VRS 17.1,
34. VRS 18.1,
35. VRS 19.1,
36. VRS 20.1,
37. VRS 21.1,
38. VRS 22.1,
39. VRS 23.1,
40. VRS 24.1,
41. VRS 25.1,
42. VRS 26.1,
43. VRS 27.1,
44. VRS 28.1,
45. VRS 29.1,
46. VRS 30.1,
47. VRS 31.1,
48. VRS 32.1,
49. VRS 33.1,
50. VRS 34.1,
51. VRS 35.1,
52. VRS 36.1,
53. VRS 37.1,
54. VRS 38.1,
55. VRS 39.1,
56. VRS 40.1,
57. VRS 41.3,
58. VRS 42.1,
59. VRS 43.1,
60. VRS 44.1,
61. VRS 45.2,
62. VRS 46.1,
63. VRS 47.1,
64. VRS 48.1,
65. VRS 49.1,
66. VRS 50.1,
67. VRS 51.1,
68. VRS 52.1
69. VRS 53.1,
70. VRS 54.1,
71. VRS 55.1,
72. VRS 56.1,
73. VRS 57.1,
74. VRS 58.1,
75. VRS 59.1,
76. VRS 60.1,
77. VRS 61.1,
78. VRS 62.1
79. VRS 63.1,
80. VRS 64.1,
81. VRS 65.1,
82. VRS 66.1,
83. VRS 67.1,
84. VRS 68.1.

Abbreviations

°	degree
°C	degree Celsius
'	minute
"	second or inch
%	per cent
1-D	one-dimensional
a	aircraft background
A	amplitude of measured HEM components
A_c, A'_c	amplitudes of calculated HEM components
A'_p	polynomial approximation of $A'_c(\delta)$
Ah	ampere hours
agl	above ground level
asl	above mean sea level
α, β, γ, a	stripping ratios
α_e, β_e , γ_e	height corrected stripping ratios
α_0	complex wave number
b	cosmic stripping factor
bgl	below ground level
BGR	Bundesanstalt für Geowissenschaften und Rohstoffe
Bi	Bismut
B_n	layer admittance
C	concentration
C_0	element concentration at ground
C_H	element concentration in presence of vegetation
CF	compact flash
ch	channel number
c_l	effective cable length
cps	counts per second
Cs	Cesium
©	copyright
d_a	apparent depth
D_a	apparent distance
DC	direct current
DEM	digital elevation model
DGPS	Differential Global Positioning System
DK	Denmark
DVD	Digital Versatile Disc
δ	inverse relative skin depth (= h/p)
δ_p	polynomial approximation of $\delta(\varepsilon_c)$
δ_T	residual (magnetics)

Δh_l	reduced laser altitude
ΔI	zero-level error of in-phase component
ΔQ	zero-level error of quadrature component
ΔT	anomalies of the total magnetic field
ΔT_f	anomalies of the total magnetic field, high-pass filtered
ΔV	diurnal (magnetic) variations
E	east
E	energy
E	ground level exposure rate
e	base of the natural logarithm ($1/e \approx 0.37$)
eTh	equivalent concentration of Thorium
eU	equivalent concentration of Uranium
EM	electromagnetic(s)
ERDF	European Regional Development Fund
EU	European Union
ε	ratio of measured HEM components (= Q/I)
ε_c	ratio of calculated HEM components (= Q/I)
ε_0	permittivity of air: 8.854×10^{-12} As/Vm
ε_n	layer permittivity
f	frequency
F	IRGF
FAS	Fugro Airborne Surveys
FFT	Fast Fourier Transform
ft	feet
G	gain constant
GBA	Geologische Bundesanstalt
GPS	Global Positioning System
h	bird altitude
H	thickness of vegetation
HCP	horizontal coplanar
h_e	effective height
h_0	nominal survey height
HEM	helicopter-borne electromagnetic(s)
HMG	helicopter-borne magnetic(s)
HRD	helicopter-borne radiometric(s)
h_GPS	GPS-Höhe
h_l	laser altitude
h_r, h_r	radar altitude
Hz	hertz
i	counter
I	in-phase component (real part) of the HEM data

I_c	calculated in-phase value
IAEA	International Atomic Energy Association
IAGA	International Association of Geomagnetism and Aeronomy
IGRF	International Geomagnetic Reference Field
J_0	Bessel function of first kind and zero order
K	degree Kelvin
K	Potassium
keV	kilo electron volts
kg	kilogram
kHz	kilohertz
km	kilometre
km/h	kilometres per hour
l	litre
log	logarithm
λ	wave number
m	metre
MeV	mega electron volts
μ	attenuation coefficient (vegetation or height)
μ_0	permeability of air:$4\pi \times 10^{-7}$ Vs/Am,
μ_n	layer permeability
µR/h	microroentgens per hour
n	number of frequencies
N	north
n, N	raw, corrected count rate
NaI	sodium iodide
NASVD	noise adjusted singular value decomposition
NL	non-linear
NL	The Netherlands
nT	nanotesla
$N_{m'}$	observed count rate at STP effective height
N_S	corrected count rate at nominal survey height
N_x	background and STP corrected count rates (x = K, U, Th)
$N_{x(corr)}$	stripping corrected count rates (x = K, U, Th)
Ωm	ohm metre (Ohm*m)
p	skin depth
P	barometric pressure
P_0	barometric pressure at sea level
PDF	Portable Document Format
ppm	parts per million
π	Pi (=3.14159265…)
Q	quadrature or out-of-phase component (imaginary part) of the HEM data

Q_c	calculated quadrature value
r	distance parameter
R_1	reflexion factor
r_l	conversion factor
ρ	resistivity
ρ_0	resistivity of air: > 10^8 Ωm
ρ_a	apparent resistivity
S	south
S	sensitivity
s	second
STE	standard error
STP	standard pressure and temperature
t	thickness (of a model layer)
t	time variable
T	air temperature
T_0	temperature at freezing point of water on Kelvin scale
T, TMI	total magnetic field intensity
tanh	hyperbolic tangent
TC	total count
Th	Thorium
Tl	Thallium
t_l	life time
T_{LP}	low pass cut-off period
U	Uranium
USA	United States of America
USB	Universal Serial Bus
UTC	Coordinated Universal Time
UTM	Universal Transverse Mercator Projection
V	volt
VCX	vertical coaxial
VRS	vertical resistivity section
W	west
WFD	Water Framework Directive
WGS	World Geodetic System
ω	circular frequency
X, Y, Z	Cartesian coordinates, Z depth axis
Z	relative secondary magnetic field
z*	centroid depth

1. Summary

Climate change simulations indicate a sea-level rise and increasing rainfall in the North Sea region leading to higher groundwater levels and a forced outwash of nutrients and pollutants from industrial areas, agriculture and landfills. CLIWAT (climate & water) is a transnational Interreg project in the North Sea region funded by the European Union with partners from Belgium, The Netherlands, Germany and Denmark. The goal of the project is to determine the effects of a possible climate change on groundwater systems, surface water and the fresh-saltwater boundary in the North Sea and Baltic Sea region.

Geological and geophysical measurements were carried out in the seven pilot areas of the project. In order to map the existing groundwater structures with airborne geophysical methods the German Federal Institute for Geosciences and Natural Resources (BGR) conducted three surveys in Zeeland, Friesland (both NL) and Vojens (DK). One of these pilot areas covers parts of northern Schleswig and southern Jutland on both sides of the Danish-German border. The target of this pilot area, the Hørløkke landfill, is located to the west of the town of Vojens in the northern part of the pilot area. The public landfill covers an area of about 12,000 m² where approximately 65,000 m³ of household and industrial waste were filled in from 1968 to 1972. As the water divide is just east of the landfill it is suspected that a rising groundwater table will divert the plume of contaminants to the east – directly towards the town of Vojens.

By request of the Danish project partner Region Syddanmark a helicopter-borne survey of the area around Hørløkke landfill was conducted by the BGR airborne group in June 2009. The airborne survey comprises a 6.5 km by 8 km wide area ranging from 9°11'49"E to 9°19'24"E and 55°13'50"N to 55°17'20"N. With 6 flights 68 E–W profile lines and 16 N–S tie lines were flown, totalling about 687 line-km. The nominal flight-line spacing was 80 m for the profile lines and 500 m for the tie lines.

The BGR helicopter-borne geophysical system includes six-frequency electromagnetics (HEM), magnetics (HMG) and radiometrics (HRD). The electromagnetic system provides information about the distribution of electrical conductivity in the earth down to a maximum depth of 150 m. The intensity of the earth's total magnetic field is measured with a magnetometer. Magnetic anomalies may have deep sources as well as shallow ones. The intensity of the gamma radiation is registered by a gamma-ray spectrometer. The radiation measured is mainly emitted from the elements thorium, uranium, and potassium. The origin of this radiation is normally close to the earth's surface.

The helicopter-borne system consists of the BGR helicopter, the geophysical equipment and electronic equipment for navigation. The HEM and HMG sensors, the GPS antenna and a laser altimeter are installed inside a towed tube, called bird. The navigation instruments and the gamma-ray spectrometer are mounted in the helicopter. A ground base station records the time-variant data required to correct the airborne data.

The survey altitudes of the sensors are normally 30–40 m for electromagnetics and magnetics and 70–80 m for gamma-ray spectrometry. HEM and HMG data are recorded 10 times per second during a survey flight and HRD data are recorded once per second. At an aircraft speed of about 140–150 km/h, this leads to mean sampling intervals of about 4 m and 40 m, respectively.

The collected geophysical data and the corresponding positioning data are stored on a CF card during the flight. The digital data are checked immediately after the flight. Further processing of all survey data, including the data of the simultaneously operating base station which records the variations of the total magnetic intensity and the variations of the atmospheric pressure, take place in the field and finally at BGR in Hanover.

This "Technical Report" describes the survey operations and the survey equipment used, as well as the data processing and the presentation of the results as vertical resistivity sections and thematic maps. The processed data, the thematic maps and the vertical sections are stored on a DVD, accompanying this report.

Following parameters are displayed on a topographic map at a scale of 1:25,000:

- actual flight lines,
- topographic elevations,
- apparent resistivities at six frequencies (387, 1,820, 5,403, 8,389, 41,430 and 133,200 Hz),
- centroid depths at six frequencies (387, 1,820, 5,403, 8,389, 41,430 and 133,200 Hz),
- resistivities at 1, 3, 5, 10, 20, 30, 50, 70, 90 and 120 m below ground level,
- anomalies of the total magnetic field,
- anomalies of the total magnetic field, high-pass filtered, anthropogenic anomalies removed,
- concentration of potassium,
- equivalent concentration of thorium,
- equivalent concentration of uranium,
- total count,
- exposure rate.

Cross-sections based on resistivity-depth 1-D inversion models (vertical resistivity sections) are displayed along all flight lines at a horizontal scale of 1:25,000 with a vertical exaggeration of 10.

2. Introduction

Climate change simulations indicate a sea-level rise and increasing rainfall in the North Sea region. This will lead to higher groundwater levels and a forced outwash of nutrients and pollutants from industrial areas, agriculture and landfills (http://cliwat.eu/). The climate changes will affect the assessment of suitable industrial and agricultural development areas due to changes in the shape of the local waterworks catchments areas. Rise in groundwater level will challenge the construction business and it will be necessary to come up with new standards. It will also change the available groundwater resource and pattern of stream flow between summer and winter (reduced potential for irrigation from water table aquifers interacting with streams).

CLIWAT (climate & water) is a transnational project funded by the Interreg IVB North Sea Region Programme of the European Regional Development Fund (ERDF) with partners from four participating countries of the European Union (EU): Belgium (Ghent University), The Netherlands (Deltares/TNO, VITENS, Provincie Fryslân, Wetterskip Fryslân), Germany (LIAG, LLUR, SEECON, BGR) and Denmark (Region Midtjylland, GEUS, Region Syddanmark, Environment Centre Aarhus, Environment Centre Ribe, Aarhus University, Municipality of Horsens).

The goal of the project is to determine the effects of a possible climate change on groundwater systems, surface water and the fresh-saltwater boundary in the North Sea and Baltic Sea region. The effect of the increased flux from agricultural and industrial land sites and landfills on groundwater quality in relation to indicators in the EU Water Framework Directive (WFD) has to be investigated as well as the impact on waterworks and important ground water aquifers near the coastlines. Also open question are the potential towards more accessible water in the hydrological system, the assessment of the consequences due to the increased recharge to groundwater systems and how to manage and solve the upcoming challenges for the construction business, for drainage and changes in conditions for biological/chemical decomposition in the soil.

Therefore geological and geophysical measurements were carried out in the seven pilot areas of the project (**Fig. 1**):

A: Belgische Middenkust, Belgium,

B: Zeeland, The Netherlands,

C: Terschelling and Northern Friesland, The Netherlands,

D: Borkum, Germany,

E: Schleswig and Southern Jutland, Germany and Denmark,

F: Egebjerg, Denmark,

G: Aarhus river, Denmark.

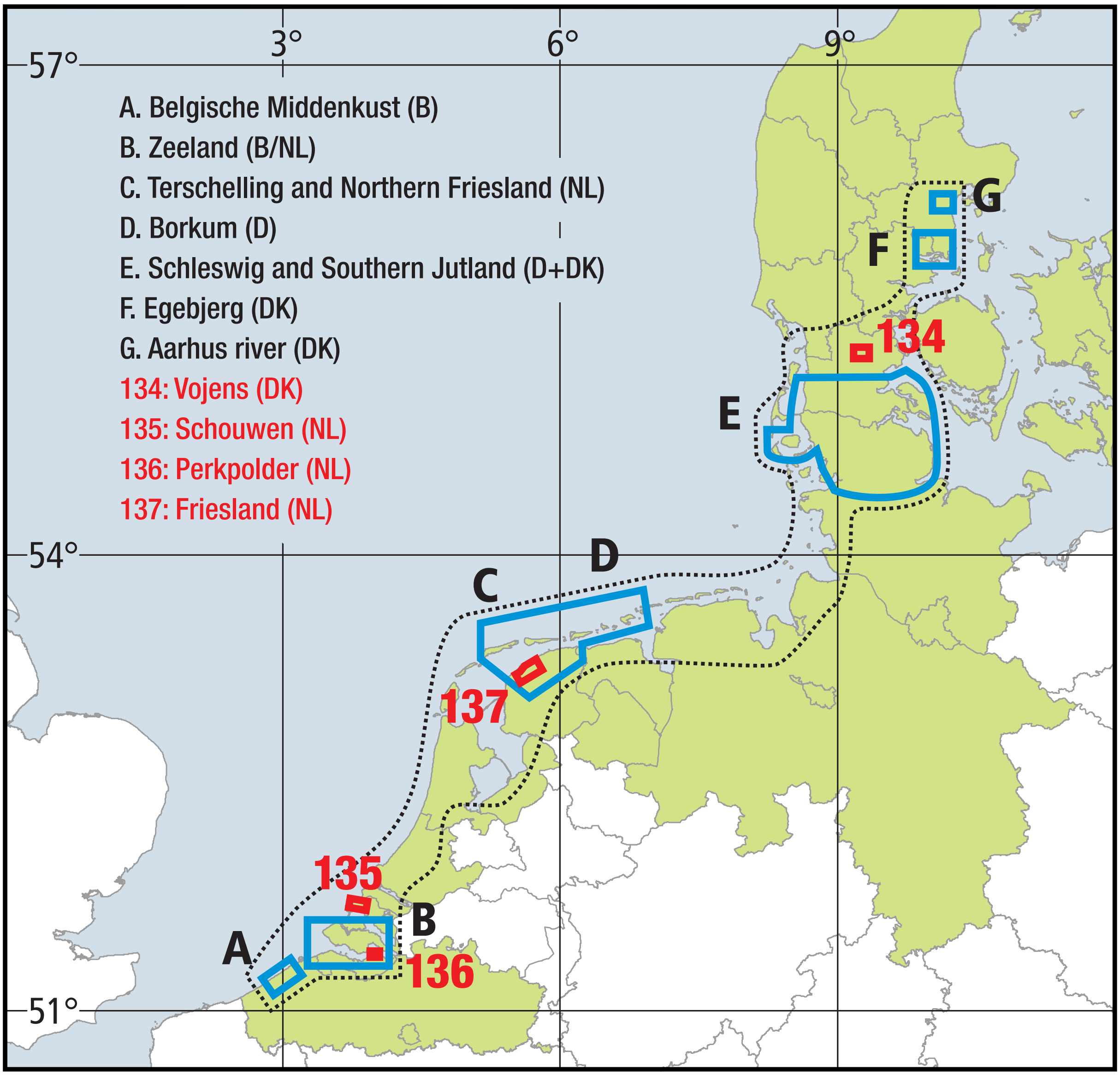

Fig. 1: *Regions (green) funded by the Interreg IVB North Sea Region Programme of the European Regional Development Fund (ERDF) and project areas A-G. Red numbers indicate the BGR airborne survey areas.*

One of these pilot areas (**E**) is located on the Danish-German border covering parts of northern Schleswig and southern Jutland (Sønderjylland). The Hørløkke landfill to the west of the town of Vojens is one of the targets belonging to this pilot area (**Fig. 2**). The public landfill covers an area of about 12,000 m^2 where approximately 65,000 m^3 of household and industrial waste were filled in from 1968 to 1972. The leaching of contaminants is a severe problem as the water divide is just east of the landfill and it is suspected that a rising groundwater table will divert the plume to the east – directly towards the town of Vojens.

A helicopter-borne survey of the area around Hørløkke landfill was conducted by the airborne group of the German Federal Institute for Geosciences and Natural Resources (BGR) in June 2009. The

Danish project partner Region Syddanmark, who is responsible for the coordination of the measurements and the interpretation of the diverse data sets of the area, requested the airborne survey.

This "Technical Report" describes the survey operations and the survey equipment in use, as well as the data processing and the presentation of the results as vertical resistivity sections and thematic maps. The processed data, the thematic maps and the vertical sections are stored on a DVD accompanying this report.

3. Survey Area

The Vojens survey area around Hørløkke landfill is situated to the northwest of the town of Vojens, Denmark. It comprises a nominal 6.5 km by 8 km wide area ranging from 9°11'49"E to 9°19'24"E and 55°13'50"N to 55°17'20"N. The actual survey area differs from the planned one due to restrictions by the Danish Civil Aviation Administration. As it was not allowed to overfly densely inhabited areas or buildings without obtaining the owner's permission, the actual flight lines deviate from the nominally straight lines where homesteads, villages and towns exist. A map of the projected survey area (small red dots) and its actual realization (bold red dots) is shown in **Fig. 2**, which also shows the boundary (dashed black line) of the 1: 25,000 topographic map used to present the geophysical results.

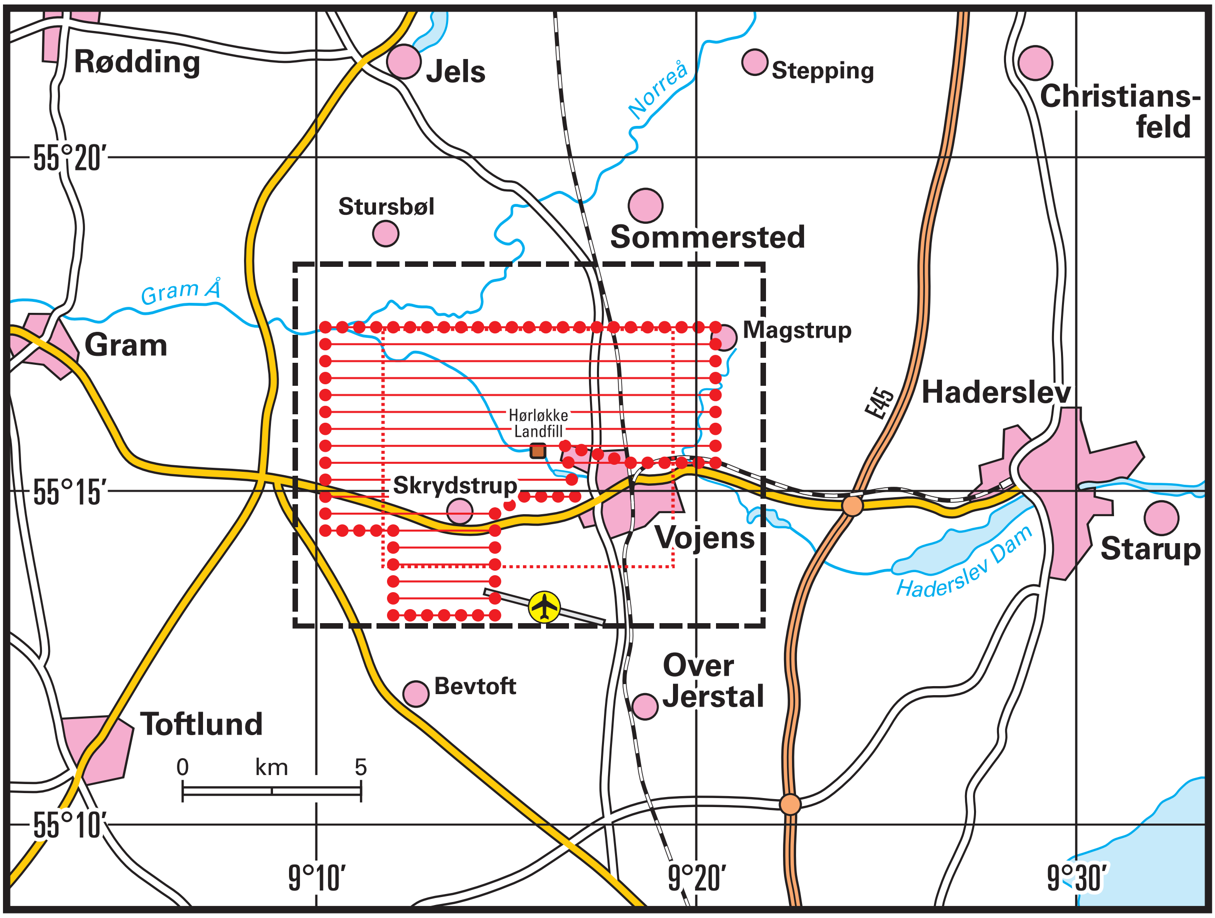

Fig. 2: *Vojens survey area (red dots), projected area (red dotted line) and the frame of the map sheet (black dashed line).*

An area of approximately 54 km² was surveyed with 6 flights on June 23–25, 2009. There were 68 E–W profile lines and 16 N–S tie lines flown, totalling about 687 line-km. The nominal flight-line spacing was 80 m for the profile lines and 500 m for the tie lines. The survey flights commenced from Vojens airport (42 m asl). The survey parameters are given in **Table 1**.

Table 1: *Survey parameters for the Vojens survey area.*

BGR area number	Vojens (DK) 134
Field period	June 23–25, 2009
Size of survey area	54 km²
Total length of survey lines	687 km
Number of survey flights	6
Flight numbers	13401–13406
Mean flight altitude of the EM sensor above ground	40 m
Speed during survey flight	140 km/h
Number of profile-line flights	4
Number of profile lines	68
Profile-line lengths	4–12 km
Profile-line directions (angle to N)	90°
Profile-line spacing	80 m
Number of tie-line flights	2
Number of tie lines	16
Tie-line lengths	3–8 km
Tie-line directions (angle to N)	0°
Tie-line spacing	500 m

The lines flown primarily northwards or eastwards are normally given an even profile number, while the ones flown in the opposite directions are odd numbered. The profile lines have the extension ".1" (after the profile number) or ".2" or ".3" for repeated lines, and the tie lines have the extension ".9" or ".8" for repeated lines. Details of the survey flights are given in **Appendix I**.

The average altitude of the helicopter was 40 m above ground level within the survey area. During a survey flight, particularly before the first and after the last profile, the altitude was increased to >350 m to check the calibration of the HEM system far from any disturbing influences.

The base station recording the magnetic variations was located on the airport at 55°13'39''N, 9°16'46''E and 43 m asl.

4. Airborne Geophysical System

BGR's airborne geophysical system simultaneously records the electromagnetic, magnetic, and gamma-ray spectrometry data. The geophysical instrumentation, the navigation and positioning systems, the digital recording units, as well as other equipment needed for the survey flights are integrated in one measuring system carried by a Sikorsky S-76B helicopter (**Fig. 3**).

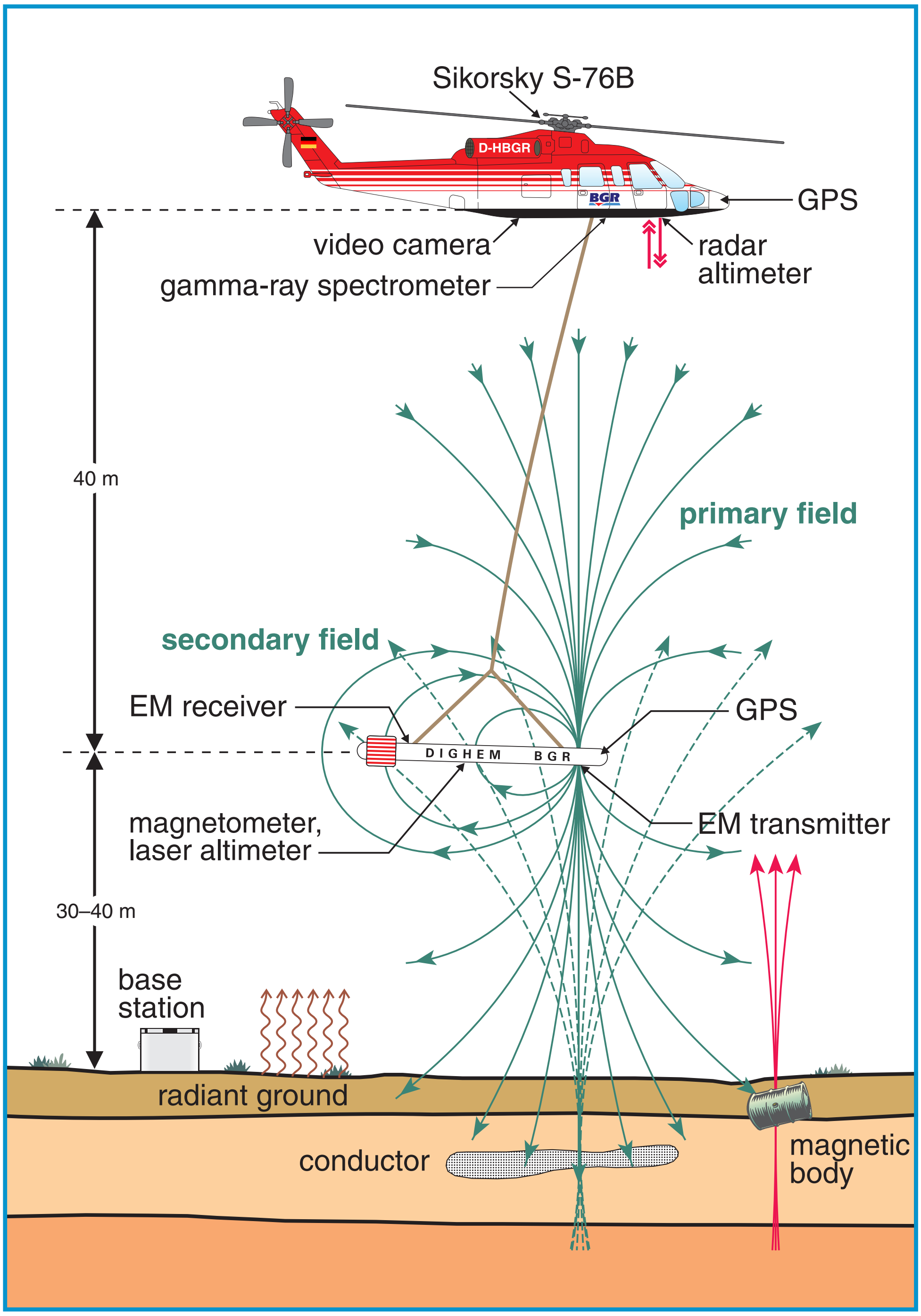

Fig. 3: *Principal sketch of the BGR airborne geophysical system.*

4.1. The Helicopter

The helicopter, a Sikorsky S-76B (see **Table 2**), was purchased in 1986 by the Federal Ministry for Economic Cooperation and Development and assigned to BGR, mainly for technical cooperation projects.

Table 2: *Technical specifications of the BGR helicopter D–HBGR*

Helicopter	
Type	Sikorsky S-76B (Manufacturer: Sikorsky, USA)
Year of manufacture	1986
Engines	2 turbines Pratt & Whitney PT6B-36A with 1033 SHP (shaft horse power) for each
Maximum gross weight	11,700 pounds (5,363 kg)
Maximum payload	3,300 pounds (1,500 kg)
Maximum flight duration	2:45 hours
Fuel consumption per hour	350–400 l

4.2. Measuring System

The airborne geophysical system (**Table 3**) is installed in the helicopter and in a towed tube, called bird. The navigation instruments and the gamma-ray spectrometer are mounted in the helicopter. The HEM and HMG sensors, the GPS antenna and a laser altimeter are installed inside the bird. This bird is towed by a 45 m long cable and its position is, depending on the flight speed, about 40 m beneath and little behind the helicopter. A ground base station records the time-variant data required to correct the airborne data.

The geophysical and recording systems are controlled by the HeliDas system that also assists the navigation during a survey flight. The operator as well as the navigator is able to check the flight data online as information about the flight path and selected data channels are displayed on tablet computers.

Table 3: *The geophysical survey system*

Geophysical systems		
Bird	**I. Six -frequency electromagnetic system (HEM)**	
	Function	Investigation of the underground electric conductivity down to a maximum depth of about 150 m
	Manufacturer	Fugro Airborne Surveys (FAS), Canada
	Type	RESOLVE, BKS36a (Bird 61)
	II. Caesium magnetometer	
	Function	Recording of the total magnetic intensity of the earth
	Manufacturer	Geometrics, USA
	Type	G-822A
Helicopter	**III. Gamma-ray spectrometer**	
	Function	Recording of the energy spectrum of natural and man-made gamma radiation within a range of 0 to 3 MeV
	Manufacturer	Exploranium, Canada
	Type	Spectrometer: GR-820; Detector crystals: GPX-1024/256

4.3. Electromagnetics

A sinusoidal current flow through a transmitter coil at a discrete frequency generates the primary magnetic field. At a distance greater than about 2 m this field is very similar to a field of a magnetic dipole located in the centre of the transmitter coil. The resulting eddy currents in the subsurface generate a secondary magnetic field that depends on the frequency used and the conductivity distribution. The difference of the fields picked up by the receiver coil and a bucking coil, which is used to cancel out the dominating primary field, is related to the primary magnetic field at the receiver coil, i. e., the quantity measured is the relative secondary magnetic field in parts per million (ppm). Due to a small phase shift between the primary and the secondary field, the relative secondary magnetic field is a complex quantity with in-phase and out-of-phase (quadrature) components.

The HEM system, RESOLVE manufactured by Fugro Airborne Surveys, utilises six individual coil systems consisting of transmitter, receiver, bucking and calibration coils. The transmitter and receiver coils have a diameter of about half a metre and a distance of about 8 m. The orientation of five transmitter-receiver coil systems is horizontal coplanar (HCP) what is suitable for groundwater exploration purposes as the induced currents are predominantly flowing horizontally resolving layered structures best. In addition, a vertical coaxial coil (VCX) system is used in order to better locate vertical structures such as fault or fracture zones. The coil systems are housed by a 10 m long tube.

Table 4: *HEM system parameters (Bird 61)*

Frequency [Hz]	Coil separation [m]	Coil orientation	Denotation FAS	Denotation BGR
387	7.938	horizontal coplanar	EM_3	1. frequency
1,820	7.931	horizontal coplanar	EM_5	2. frequency
5,403	9.055	vertical coaxial	EM_6	3. frequency
8,389	7.925	horizontal coplanar	EM_2	4. frequency
41,430	7.912	horizontal coplanar	EM_1	5. frequency
133,200	7.918	horizontal coplanar	EM_4	6. frequency

Small coils placed in the centre of each receiver coil are used for calibration. The calibration factors necessary to convert the measured signals to ppm values were provided by the manufacturer. The in-phase and quadrature components of the relative secondary magnetic fields are used to derive the three-dimensional distribution of the electrical conductivity – or its inverse, the resistivity – in the subsurface. Horizontal resolution and vertical resolution are achieved by moving the system and using different system frequencies, respectively. Due to the skin-effect (high frequency currents are flowing on top of a perfect conductor) the penetration depths of the electromagnetic fields increase with decreasing frequency and conductivity. The frequencies used range from 387 Hz to 133 kHz enabling exploration depth ranges of about 1-30 m in a very conductive host such as saltwater saturated sediments and 5-150 m in a rather resistive host such as freshwater saturated sandy sediments.

The HEM system is not only sensitive to the electrically conductive subsurface but also to anthropogenic objects like, e. g., buildings, metallic bodies, and electrical installations, which have influence on the data measured, particularly at lower frequencies. As the helicopter itself is such an object, the HEM system is towed at a sufficiently large distance (about 40 m) underneath the helicopter.

4.4. Magnetics

A highly sensitive caesium vapour magnetometer installed in the bird is used to measure the total intensity of the earth's magnetic field (unit Nanotesla, nT). The function of a caesium magnetometer is based on the measurement of the so-called Larmor frequency that occurs in a special, optically pumped system in the sensor. The frequency is directly proportional to the magnetic field intensity and can be determined with high precision and accuracy. The resolution of the instrument is 0.01 nT.

The magnetic field measured is composed of different parts. The Earth's main field, caused by sources in the Earth's core, varies between approximately 20,000 nT in equatorial regions and 70,000 nT at the poles. It is superimposed by the crustal magnetic field caused by rocks containing magnetised minerals. These produce anomalies in the range between less than one and up to several hundred nT. In populated areas, anthropogenic sources such as buildings, industrial plants, power lines, etc. can produce additional locally confined and sometimes strong magnetic anomalies. Finally, the magnetic field is subject to temporal changes due to fluctuations in the state of the ionosphere and magnetosphere. These diurnal variations are in the order of several tens of nT.

In order to record the diurnal variations, a magnetic base station (**Table 5**) is operated. The station, also equipped with a caesium magnetometer, is installed close to the area of investigation in a magnetically undisturbed place. Data recorded by the base station during the survey are used to correct the total magnetic field measured during the flight. GPS time is used to synchronise the two data sets.

Table 5: *Base station*

Base station	
Magnetic base station	
Function	Recording of the variation of the total magnetic intensity (TMI)
Manufacturer	Base station: FAS, Canada Magnetometer: Cs sensor H-8, SCINTREX, Canada
Type	CF1 Data Logger

4.5. Radiometrics

For geophysical investigations the count rates of the common terrestrial radioactive elements (or their isotopes and daughter products) Tl-208 (thorium series), Bi-214 (uranium series), K-40 (potassium) are of interest. Mapping of the distribution of these three elements in the ground are useful for geological investigations.

BGR uses a standard 256-channel spectrometer system consisting of four sodium iodide (NaI) crystals to detect the ground gamma radiation and one upward looking crystal to detect the radon radiation in the air. The spectrometer crystals are placed together in an aluminium box. Each crystal has a volume of approximately 4 l ($0.1 \times 0.1 \times 0.4$ m^3). Incident gamma radiation is absorbed by the crystals and transformed to light pulses that are converted to electric pulses using a photomultiplier tube. The amplitudes of the electric pulses are directly proportional to the energy of incident gamma radiation.

The spectrometer covers an energy spectrum from 0 to 3 MeV. Depending on their energy, the pulses are mapped into one of 255 energy channels. Channel 256 is reserved for recording cosmic radiation between 3 and 6 MeV. Spectra recorded by the system contain counts of gamma radiation collected and integrated over one second. Energy windows and channel ranges of the different radiation sources are listed in **Table 6**. The spectrometer is internally stabilised for possible drifts in gain. This is done independently for each of the four downward-looking crystals using the thorium peak. Shifts of the thorium peak (2.62 MeV) relative to the nominal value are identified and the gain of the photomultiplier tube of the respective crystal is corrected automatically. A caesium sample is used to stabilize the gain of the upward looking crystal.

Table 6: *Radiation sources and corresponding spectrometer parameters*

Radiation source	Energy window in MeV	Peak energy in MeV	Channel range
Total count	0.41–2.81	—	34–233
Potassium (K-40)	1.37–1.57	1.46	115–131
Uranium (Bi-214)	1.66–1.86	1.76	139–155
Thorium (Tl-208)	2.41–2.81	2.62	202–233
Cosmic radiation	3.0–6.0	—	255

4.6. Navigation and Positioning

The navigation system (**Table 7**) provides the pilot with all the information necessary to carry out a survey flight. Navigation software (LiNav von AG-NAV Inc.) calculates the coordinates of the starting and the end points of all survey lines from the coordinates of the corners of the survey area, the profile direction and the spacing of the flight lines. These coordinates are copied to the HeliDas system using a CF card or an USB stick. These profiles are displayed on the tablet computer with the line being flown highlighted.

Table 7: *Navigation and positioning systems*

Systems for navigation and positioning		
Helicopter	**Navigation system**	
	Function	On-line determination and display of the GPS navigational data required by the pilot during a survey flight; recording of the geographic position of the helicopter and its altitude above mean sea level
	Manufacturer	Navigation computer and display: FAS, Canada GPS receiver: NovAtel, Canada
	Type	Navigation computer: HeliDas GPS receiver: NovAtel OEMV-2-L1/L2 GPS antenna: NovAtel L1/L2 ANT-532-e
Bird	**Positioning system**	
	Function	Determination and recording of the geographic position of the HEM bird and its altitude above mean sea level
	Manufacturer	Position recording and display: FAS, Canada GPS receiver: CSI Wireless, Canada
	Type	Position recording: HeliDas GPS receiver: DGPS MAX

The pilot obtains all information required to fly this profile as accurately as possible from a second display. The most important information is the lateral deviation from a line. The deviation appears digitally in metres, as well as on a bar diagram. The navigation computer receives information about the position of the helicopter from a GPS navigation receiver whose antenna is fixed outside on the helicopter. The error in the navigation data is less than 1–2 m.

The positioning system (**Table 7**) provides the coordinates of each geophysical measurement. A second GPS navigation receiver is used for this purpose, whose antenna is fixed inside the bird. The spatial positions of the sensors are determined from this positioning data. The error of the coordinates is also in the order of 1–2 m.

A radar altimeter (**Table 8**) attached to the bottom of the helicopter determines its altitude above the ground or above obstacles (e. g., large stands of trees and buildings) with a precision of ±3 m. The altitude is needed to process the radiometric data. A barometric altimeter is used to determine the altitude of the helicopter above mean sea level, but this altimeter is employed only as a backup for the GPS receivers. Without a base station as reference the GPS measurements may have an error of some metres.

The altitude of the bird above the ground must be accurately known for the processing of the electromagnetic data and to generate a digital terrain model. A laser altimeter (**Table 8**) inside the bird provides this altitude with a precision of ±0.2 m. A further advantage of the laser altimeter, in addition to its precision, is the focused laser beam, which when above a forest often allows the distance to the surface to be determined and not only to the treetops, as it is the case with the radar altimeter.

Table 8: *Altimeters*

Altimeters		
Helicopter	**Radar Altimeter**	
	Function	Recording of the altitude of the helicopter above ground level
	Manufacturer	Sperry, USA
	Type	AA-200
	Barometric Altimeter	
	Function	Recording of the altitude of the helicopter above mean sea level
	Manufacturer	Rosemount, USA
	Type	1241A5B
Bird	**Laser Altimeter**	
	Function	Precise recording of the altitude of the HEM bird above ground
	Manufacturer	Riegl, Austria
	Type	LD90-3800VHS

The digital elevation model is derived from the GPS elevation of the HEM bird in m asl minus the laser altitude. Without a base station as reference for the GPS measurements, and thus, the topographic elevations may have an error of some metres.

4.7. Data Acquisition and Recording

The HeliDas system stores all the data digitally on CF card during a survey flight (**Table 9**). The data sets are ready for processing with GEOSOFT OASIS montaj. The most important data channels are also displayed on the tablet computers to enable continual checking of the data during the flight. Immediately after a flight, the digital data are copied to a field computer and checked more accurately in order to obtain an impression of the geophysical results and to detect any problems with the survey system.

Table 9: *Data acquisition and recording systems*

	Data acquisition and recording systems	
Helicopter	**Function**	Digitizing of the analogue signals, buffering of all digital data; flight path and displaying of selected data channels; storage of position and field data on CF card ready for processing with GEOSOFT OASIS montaj
	Manufacturer	FAS, Canada
	Type	HeliDas

4.8. Video System

A video camera (**Table 10**) is mounted in the bottom of the helicopter. Two monitors, one in the cockpit and one in the operator's rack, allow monitoring of the bird at take-off and landing as well as during the flight.

The video recording of the flight path is used to locate sources of anomalous or disturbed data on the ground. The flight path video can be correlated directly with the digital data.

Table 10: *Video system*

	Video system	
Helicopter	**Function**	Recording of the flight track and monitoring of the movements of the HEM bird during take-off, landing and flight
	Manufacturer	Colour camera: Sony, Japan Video recorder: AXI, Sweden
	Type	Colour camera: DC372P Video server: AXIS 241S

4.9. Additional Equipment

The 28 V DC on-board voltage of the helicopter is smoothly buffered by a 24 Ah battery and connected to a central power unit. From there it is distributed to the individual components of the system with fuses built-in to protect devices from overvoltage.

Control and recording units of the airborne geophysical system are mounted in a 19'' rack. Shock absorbers between the base of the rack and a wood board which is firmly screwed to the floor of the helicopter minimize the transfer of vibrations originating from the rotor.

Table 11: *Additional equipment*

Additional equipment		
Helicopter	**Central power unit**	
	Function	28 V DC on-board voltage of the helicopter buffered by a 24 Ah buffer battery and connected to a central power unit
	Manufacturer	Sikorsky, USA
	Instrument rack	
	Function	19'' rack on shock absorbers to mount all components of the airborne geophysical system
	Manufacturer	Sikorsky, USA

5. Processing and Presentation of the Survey Data

The general objectives of the data processing may be summarized as follows:

- quality control of the measured data;
- conversion of the field data into physical parameters;
- presentation of the results as maps and vertical sections.

5.1. General Processing Steps

The airborne geophysical data are copied from the CF card to field computers directly after a survey flight in order to save the data and to check them for plausibility and for correctness. Using the software GEOSOFT OASIS montaj, the primary field data processing steps are conducted automatically, followed by a pre-processing of all survey data in order to display preliminary results.

The final data processing starts with the processing of the position data:

- coordinate transformation;
- correction of altitude data of the helicopter and the bird.

The following processing steps are valid for all methods:

- removal of spiky data;
- reduction of high-frequency noise by digital filtering;
- conversion of the data to the desired geophysical parameters;
- fixing of the ends of the profiles;
- merging the flight-line data sets to area data sets;
- levelling of the data;
- storage of the final survey data and geophysical parameters;
- production of maps and vertical sections (only HEM).

The field data processing and the calculation of the physical parameters for each method are described in more detail in the following chapters. GEOSOFT OASIS montaj is used throughout if not otherwise noted.

5.2. Position Data

5.2.1. Coordinates

The coordinates of the helicopter and the bird recorded during the survey flight refer to the WGS 84 geographic coordinate system. These geographic coordinates are transformed to local Cartesian coordinates. False coordinates are corrected und gaps are interpolated.

All survey results refer to UTM WGS 84 coordinates (9° meridian, zone 32N).

5.2.2. Radar Altitude

The radar altitude data measured in feet at the helicopter (h_r_{mess}) have to be transformed to metres above ground level (m agl). For the purpose of comparison with the laser altitude data of the bird (h_l), the radar altitudes are also referred to the bird altitude (h_r)

$$h\_r\,[m] = h\_r_{mess}\,[feet] \cdot 0{,}3048\,[m/feet] \cdot r_l - c_l\,[m],$$

where

h_r [m]	=	adjusted radar altitude (unit: m agl),
h_r_{mess} [feet]	=	radar altitude (unit: feet) measured by the altimeter,
r_l	=	conversion factor (gradient),
c_l	=	effective cable length (offset).

For this, the effective cable length, i. e., the distance between the helicopter and the bird, has to be estimated and subtracted. The effective cable length can be derived from the differences of the GPS elevations of the helicopter and the bird. Alternatively, the effective cable length and the conversion factor r_l of laser and radar altitudes are obtained by linear regression.

For the correction of the radar altitude data r_l = 1.04 and c_l = 44 m were used.

5.2.3. Laser Altitude

The laser altimeter data representing the bird altitude – as well as the radar altimeter data – may have gaps and outliers which have to be corrected by elimination and interpolation procedures. The movement of the bird causes attitudes (pitch and roll) deviating from the normal case and, thus, laser altitudes which are normally higher than the actual bird altitude. The mean pitch angle of about 6° is corrected by applying the corresponding cosine function. The roll angle is generally not known. Thus, after identification by comparison with the radar altitudes of the bird, strongly affected laser altitudes have to be eliminated and interpolated afterwards.

The measurements of the laser altimeter data may be affected by the tree canopy or other reflectors. Thus, the distance between the helicopter containing the radiometric system or the bird containing the electromagnetic and magnetic systems and the ground level is often not correctly measured resulting in laser altitudes which are too low.

The affected laser altitudes (h_l) are corrected with the help of a combination of several checks and filter techniques (**Table 12**). The first step is to reduce the effect of strong gradients in the laser altitudes due to rapid changes in bird or topographic elevation. A base line derived by applying a low-pass filter to the laser altitude data is subtracted from the laser altitude data to calculate reduced laser altitude values (Δh_l). Remaining outliers are removed by applying a very short non-linear filter. In order to identify and eliminate those segments where trees or other obstacles exist, two procedures are applied to the reduced laser altitude data:

a) Noise filter, followed by non-linear and low-pass filters applied to the noise channel (Δh_l_{noise}), and a high-noise threshold of 0.4 m;
b) Maximum filter and difference threshold of 2 m of filtered (Δh_l_{max}) and unfiltered (Δh_l) data.

The gaps of eliminated data are filled in with slightly shifted maximum values representing the corrected reduced laser altitudes. As the maximum values may be too high, their levels are shifted to the levels on both side of each gap. Finally, the corrected values are low-pass filtered (Δh_l_{kor}) and the base line is added again to get the corrected laser altitude values (h_l_{kor}). This procedure is able to eliminate all effects caused by single or small groups of trees. The effect of broad and densely wooded areas, however, is not always removed sufficiently and has to be corrected manually.

Table 12: *Filter parameters for the removal of the tree-canopy effect*

Type of filter	Filter parameters	Channel
Low pass	Cut-off period: 5 s (≈ 200 m)	h_l
Non linear	Window length: 1 point (≈ 5 m), tolerance: 1.0	Δh_l
Noise (normal distr.)	Window length: 7 points (≈ 28 m)	Δh_l
Non linear	Window length: 3 points (≈ 15 m), tolerance: 1.0	Δh_l_{noise}
Low pass	Cut-off period: 1 s (≈ 40 m)	Δh_l_{noise}
Threshold	Cut-off value (Δh_l_{noise}): 0.4 m	Δh_l
Maximum	Window length: 21 points (≈ 84 m)	Δh_l
Threshold	Cut-off value ($\Delta h\_l_{max} - \Delta h\_l$): 2 m	Δh_l
Low pass	Cut-off period: 3 s (≈ 120 m)	Δh_l_{kor}

5.2.4. Topographic Elevation

The topographic relief derived by the difference of the GPS based bird elevation and the corrected laser altitude

$$\text{topo [m asl]} = \text{h\_GPS [m asl]} - h\_l_{kor} \text{ [m]}$$

is used to derive a digital elevation model of the survey area. As the tree canopy effect causes laser altitudes which are too low, the topographic elevations are too high. Therefore, the topographic values are also useful to identify and manually correct the laser altitude for remaining tree canopy effects, particularly if external topographic data as reference are available.

In order to remove line effects the topographic elevation data were levelled with respect to the digital elevation model provided by the project partner.

5.3. Processing of the Electromagnetic Data

The processing of the measured I and Q values (in ppm), i. e., the real part (in-phase or 0°-phase) and the imaginary part (out-of-phase, quadrature or 90°-phase) of the relative secondary field requires several steps:

- application of calibration factors;
- zero-level and drift correction;
- data correction;
- transformation to half-space parameters;
- correction of man-made effects;
- levelling;
- interpolation and smoothing.

While the half-space parameters, apparent resistivity and the centroid depth, are individually derived from secondary field values for each frequency, the final resistivity models are calculated at each survey point by 1-D inversion of the data of all (or selected) frequencies.

5.3.1. Calibration of the HEM System

The HEM system was calibrated on highly resistive ground by the manufacturer in Mountsburg Conservation Area, Canada. After adjusting the phase with the help of a ferrite rod, well-defined external calibration coils were used to derive the ppm values of the internal calibration coils. These calibration factors are used to convert the voltages measured during a survey flight to ppm values representing the secondary magnetic fields (**Table 13**).

Table 13: *Calibration factors of the HEM system*

Frequency [Hz]	Calibration factors Fugro		Calibration factors BGR	
	I [ppm]	Q [ppm]	I [ppm]	Q [ppm]
387	-205.3	-205.3	-209.8	-210.8
1,820	-175.4	-174.7	-174.7	-174.3
5,403	76.6	76.8	81.9	81.2
8,389	-144.4	-144.2	-209.4	-198.8
41,430	-667.3	-665.2	-657.4	-664.9
133,200	-1404.2	-1406.4	-685.5	-911.0

At the beginning of each survey flight and at high flight altitude, phase and gain of the EM system are adjusted automatically for each frequency using internal calibration coils. Due to instrumental drift, the calibration has to be checked several times during the flight. The calibration signals caused by internal calibration coils are compared with known calibration signals and phase shifts and gain correction factors are applied to the data.

As a mutual coupling with the subsurface during the ground calibration procedure and technical changes of the system caused modified calibration factors, a flight over highly conductive North Sea water in February 2009 was used to check the calibration values. The evaluation of this data set yielded a set of phase and gain corrections being enormous particularly for the 8.3 and 133 kHz frequency data (**Table 13**).

A further check of the calibration factors during the Zeeland survey in August 2009 yielded an updated set of mean phase and gain corrections (8.3 kHz: 2% gain, 41 kHz: 0.5° phase and 133 kHz: 7° phase and 16% gain). In addition, a fine tuning of the phase and gain correction values was necessary for the highest frequency data of the Vojens survey.

5.3.2. Zero-Level and Drift Correction

The signals measured by the receivers may still contain some non-compensated parts of the primary fields generated by the transmitters. These so called zero levels may also have thermal drift. The zero levels of the HEM data are generally determined at high flight altitudes (>350 m) several times during a survey flight as the ground response is negligible at this altitude, i. e., the secondary field should be close to zero. Zero-level reference points are set at such high-altitude profile segments, preferably where the signal is not noisy. The zero level is obtained individually for each data channel by linear interpolation of the picked values at adjacent zero level reference points.

This procedure enables to remove the long-term, quasi-linear drift. Short-term variations, however, caused by temperature changes due to altitude variations, which occur particularly in the highest-frequency data, cannot be corrected successfully by this procedure. Therefore, additional reference points – also along the profiles at normal survey flight altitude – have to be determined where the secondary fields are small but not negligible. At these locations, the estimated half-space parameters are used to calculate the expected secondary field values, which then serve as local reference levels (Siemon, 2009). As this drift correction procedure is often not sufficient, statistical levelling procedures have to be applied in addition (see **Section 5.3.6**).

5.3.3. Data Correction

Noise from external sources (e. g., from radio transmitters, power lines, sferics, built-up areas, streets, railway tracks) is eliminated from the HEM data by appropriate filtering or interpolation. All those field values (I or Q) are automatically eliminated which fall below the relative standard error (rel. STE = STE/Mean) of the field values within a given data window. The field values are smoothed using a combination of non-linear (Naudy & Dreyer, 1968) and low-pass filters to exclude outliers and to suppress high-frequency noise, respectively. Due to frequency dependent data qualities the data channels are treated individually (**Table 14**).

Induction effects from buildings and other electrical installations (see **Section 5.3.5**) or effects from strongly magnetized underground sources are normally not erased from the data during the initial stage of data processing.

Table 14: *Filter parameters for HEM data processing*

Frequency [Hz]	Mean / STE [Values]	Threshold (I/Q) of rel. STE	NL filter Values/Tolerance	LP filter T_{LP} [Values]
387	75 / 25	0.06 / 0.04	20 / 3.0	40
1,820	75 / 25	0.05 / 0.05	20 / 2.0	30
5,403	75 / 20	0.05 / 0.05	10 / 2.0	30
8,389	75 / 15	0.05 / 0.05	10 / 2.0	30
41,430	75 / 15	0.05 / 0.05	5 / 2.0	30
133,200	75 / 15	0.04 / 0.02	5 / 2.0	30

5.3.4. Conversion of the Secondary Field Values to Half-Space Parameters

The relative secondary magnetic field Z = (I_c, Q_c) for a horizontal-coplanar (HCP) coil pair with a coil separation r and at an altitude h above the surface are calculated by (e.g. Ward & Hohmann, 1988)

$$Z = r^3 \int_0^\infty R_1(f,\lambda,\rho,\mu,\varepsilon) \frac{\lambda^3 e^{-2\alpha_0 h}}{\alpha_0} J_0(\lambda r)\, d\lambda$$

where $\alpha_0^2 = \lambda^2 - \omega^2\mu_0\varepsilon_0 + i\omega\mu_0/\rho_0$ with $\mu_0 = 4\pi * 10^{-7}$ Vs/Am, $\varepsilon_0 = 8.854 * 10^{-12}$ As/Vm and $\rho_0 > 10^8$ Ωm, J_0 is Bessel functions of first kind and zero order, and R_1 is the complex reflection factor containing the material parameters of the subsurface. This complex integral is evaluated numerically using fast Hankel transforms (e. g. Anderson, 1989, Johansen & Sørensen, 1979). A similar formula exists for a coaxial coil (VCX) configuration yielding smaller ppm values (VCX ≈ -0.25 * HCP). Following Weidelt (1991) the reflection factor R_1 for a N-layer half-space model is derived by a recurrence formula

$$R_1 = \frac{B_1 - \alpha_0\mu/\mu_0}{B_1 + \alpha_0\mu/\mu_0}$$

with

$$B_n = \alpha_n \frac{B_{n+1} + \alpha_n \tanh(\alpha_n t_n)}{\alpha_n + B_{n+1}\tanh(\alpha_n t_n)} \quad n = 1,2,\ldots,N-1 \quad \text{and} \quad B_N = \alpha_N$$

$$\alpha_n = \sqrt{\lambda^2 - \omega^2\varepsilon_n\mu_n + i\omega\mu_n/\rho_n} \quad n = 1,2,\ldots,N$$

where ρ_n, ε_n, μ_n and t_n are resistivity, dielectric permittivity, magnetic permeability and thickness of the n^{th} layer, respectively (t_N is assumed to be infinite). As magnetic effects and displacement currents are negligible, i. e., $\mu_n = \mu_0$, and $\varepsilon_n = \varepsilon_0$ only resistivities and depths are taken into account (**Fig. 4**).

Calculated secondary field values I_c and Q_c (in ppm) are used to convert the calibrated measured values (I and Q) to the parameters of a homogeneous half-space (Siemon, 2001),

- apparent resistivity ρ_a [Ωm] and
- apparent distance D_a [m] from the sensor to the top of the conducting half-space,

individually for each frequency.

For this, the reduced amplitude $A'_c = (h/r)^3 \cdot A_c$ with $A_c = (I_c^2+Q_c^2)^{1/2}$ and the ratio $\varepsilon_c = Q_c/I_c$ are calculated for an arbitrary half-space as a function of the ratio $\delta = h/p$ of sensor altitude h and skin depth $p = 503.3 \cdot (\rho_a/f)^{1/2}$.

The half-space parameters are then derived for each pair of measured secondary field values from the functions $A'_c(\delta)$ and $\delta(\varepsilon_c)$ approximated by polynomials ($A'_p(\delta)$ and $\delta_p(\varepsilon)$):

$$D_a = r\,(A'_p(\delta_p(\varepsilon)/A))^{1/3} \quad \text{and} \quad \rho_a = 0.4\,\pi^2\,f\,(D_a/\delta_p(\varepsilon))^2.$$

The calculated distance D_a may differ from the observed HEM sensor altitude (in m above ground level), i. e., the top of the conducting half-space model needs not to coincide with the surface of the earth as determined by the altimeters. The difference between the two quantities is defined as the apparent depth $d_a = D_a - h$. If d_a is positive, a resistive cover is assumed above the half-space. If d_a is negative, a conductive cover is assumed.

In addition to the apparent resistivity ρ_a and apparent distance D_a, the centroid depth $z^* = d_a + p/2$ is determined (Siemon, 2001). The centroid depth is a measure of the mean penetration of the induced underground currents. The resulting sounding curves, $\rho_a(z^*)$, provide the initial approximation of the vertical resistivity distribution.

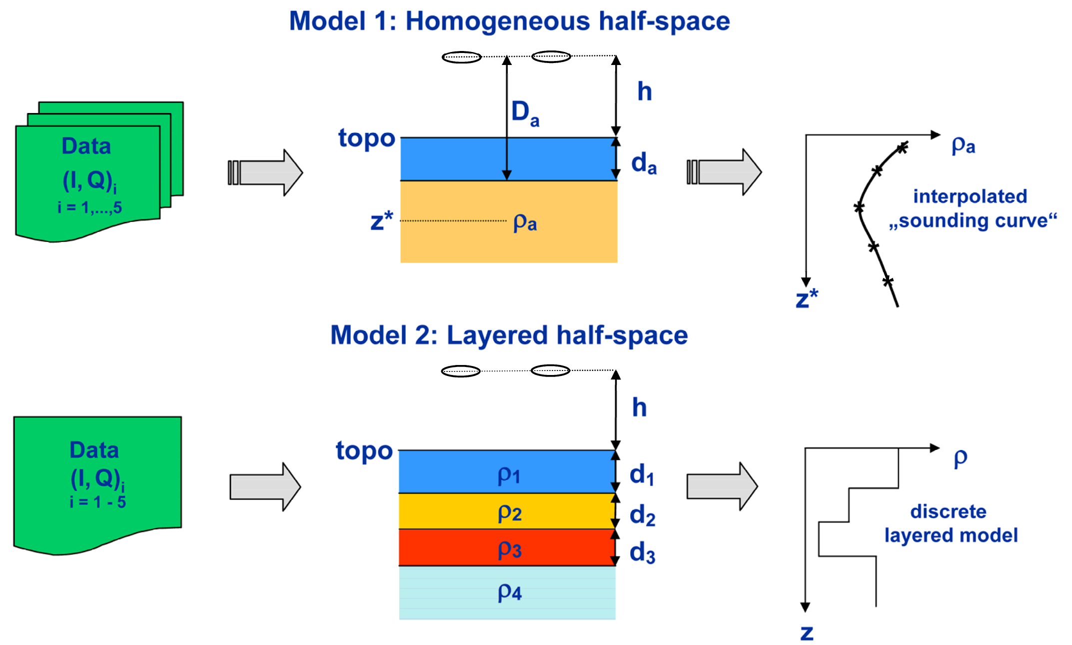

Fig. 4: *HEM inversion based on a homogeneous half-space or a layered half-space*

The actual approach for calculating the half-space parameters differs from that described by Siemon (2001) as the field values are calculated more accurately, particularly at higher frequencies, and the polynomial approximation of the functions A'(δ) und δ(ε) are optimised for each individual frequency.

The half-space parameters are checked for plausibility, i. e., high altitude (h > 100 m) and extreme (ρ_a > 1000 Ωm, d_a > 100 m) values have been eliminated, before they are used for further processing.

5.3.5. Effect of Anthropogenic Influences on the HEM Data

In addition to the geogenic contribution to the secondary fields measured over densely populated areas, there is often an anthropogenic contribution from buildings and electrical installations etc. Generally, these have little influence on the HEM data and the data can be corrected using the standard data processing tools. In some cases, e. g., large buildings with a high metal content, the anthropogenic components in the HEM data are no longer negligible. Furthermore, external electromagnetic fields exist close to power lines, electric railway tracks or built-up areas which are able to substantially affect the HEM measurements. These man-made effects appear particularly in the lower frequency data because the geogenic contribution to the secondary fields is comparatively smaller at lower than at higher frequencies and, thus, the anthropogenic contribution, which is rather frequency independent, may dominate.

The anthropogenic influence lowers the calculated resistivity and associated depth. Thus, low resistivity and depth pattern on maps and sections often correlate with man-made effects such as villages or streets. These man-made effects can be detected in the HEM data due to their typical shape or by correlation with magnetic data. Topographic or Google Earth maps of the survey area, an analysis of the video records or an on-site inspection can help identify such effects.

A manual correction of man-made effects is very time consuming as each HEM channel of each survey line has to be examined individually. Therefore, a semi-automatic filter procedure has been developed and integrated into GEOSOFT OASIS montaj software. This procedure uses the gridded data of the half-space parameters apparent resistivity and apparent depth. These grids are inspected (once or several times) for each individual frequency for anomalous data. Minimum and/or maximum anomalies are detected when the differences of the grid values and their corresponding median values, which are calculated in circular areas shifted over the grid, exceed a given threshold (**Table 15**).

Table 15: *Filter parameters for semi-automatic identification of man-made effects*

Frequency [Hz]	Radius [m] log ρ_a / d_a	Threshold log ρ_a / d_a	Number of passes log ρ_a / d_a	Type of anomaly log ρ_a / d_a
387	100 / 10	0.17 / 3	4 / 1	Min. / Min.
1,820	80 / 10	0.15 / 5	1 / 1	Min. / Both
5,403	50 / 10	0.10 / 5	1 / 1	Min. / Min.
8,389	50 / 10	0.10 / 6	1 / 1	Min. / Min.
41,430	50 / 5	0.15 / 6	2 / 1	Min. / Min.
133,200	50 / 5	0.35 / 6	7 / 1	Min. / Min.

A topographic map and a Google Earth map are used to check whether the corresponding data segments are affected due to man-made sources and – if necessary – the data are reinstalled in manually selected areas. In order to close the remaining data gaps one can either apply gridding and resampling tools on the grids or use a spline interpolation along each survey line. Afterwards the HEM data are recalculated from the corrected half-space parameters. The measured HEM data are replaced by the calculated HEM data where the semi-automatic procedure has cut the data out.

5.3.6. Statistical Levelling

In order to identify and to correct zero-level errors in the HEM data a grid based micro-levelling (**Table 16**) is applied to the half-space parameters (log ρ_a and d_a) of the parallel survey lines. The resulting error grids are resampled along the survey lines and the smoothed (spline filter: smoothness = 1.0, tension = 0.5) error channels are subtracted from the half-space parameters.

Table 16: *Filter parameters for micro-levelling of log ρ_a and d_a*

Frequency [Hz]	Butterworth (high pass) Cut-off value, degree of filter log ρ_a / d_a	Directional Cosine (pass) Azimuth, degree of function log ρ_a / d_a
387	333 m, 8 / 333 m, 6	90°, 2 / 270°, 1
1,820	500 m, 8 / 333 m, 6	90°, 2 / 270°, 2
5,403	333 m, 10 / 333 m, 6	90°, 2 / 270°, 2
8,389	333 m, 10 / 400 m, 8	90°, 2 / 270°, 2
41,430	333 m, 12 / 400 m, 8	90°, 2 / 270°, 2
133,200	333 m, 10 / 400 m, 8	90°, 2 / 270°, 2

Strong HEM anomalies are normally smoothed by the two-dimensional lateral filtering of the micro-levelling procedure. Therefore, grids where the local anomalies have been removed beforehand are used for micro-levelling, resulting in rather smooth apparent resistivity and apparent depth maps.

The tie lines are levelled afterwards using the levelled line grids as reference. The smoothed (low-pass filter: cut-off period = 50 s, wave length ≈ 2000 m) differences of levelled and unlevelled half-space parameters are used to correct the tie-line data.

The levelled half-space parameter values are then converted to secondary field values (I_c, Q_c) which are compared with the corresponding unlevelled values. Selected parts of the differences of the levelled and unlevelled values ($\Delta I = I - I_c$, $\Delta Q = Q - Q_c$) are strongly smoothed using a non-linear filter and a smoothing spline interpolation. The selection is based on constant (data noise, system altitude) and dynamic (I_{spline}, Q_{spline}) threshold values (**Table 17**). These interpolated smoothed differences are assumed to characterize the zero-level errors and they are used to correct the HEM data without losing details (Siemon, 2009). The levelling is done prior to the 1-D inversion of the HEM data.

Table 17: *Filter parameters for the levelling of HEM data*

Type of filter	Filter parameters	Channel
Threshold	Cut-off value (h_l_{kor}): 300 m	ΔI, ΔQ
Threshold	Cut-off value (I_{noise} , Q_{noise}): 0.05	ΔI, ΔQ
B-Spline	Smoothness = 1.0, tension = 0.2	I, Q
Non linear	Window length: 50 points (≈ 200 m), tolerance: 3.0	ΔI, ΔQ
B-Spline	Smoothness = 0.95, tension = 0.5	ΔI, ΔQ

5.3.7. 1-D Inversion of the HEM Data

The model parameters of the 1-D inversion are the resistivities ρ and thicknesses t of a layered half-space (**Fig. 4**), where the thickness of the underlying half-space is assumed to be infinite. Marquardt's inversion procedure is used (Sengpiel & Siemon, 2000), which requires a starting model. This starting model is derived from the apparent resistivity vs. centroid depth values $(\rho_a, z^*)_i$, i = 1,…,n (**Fig. 5**).

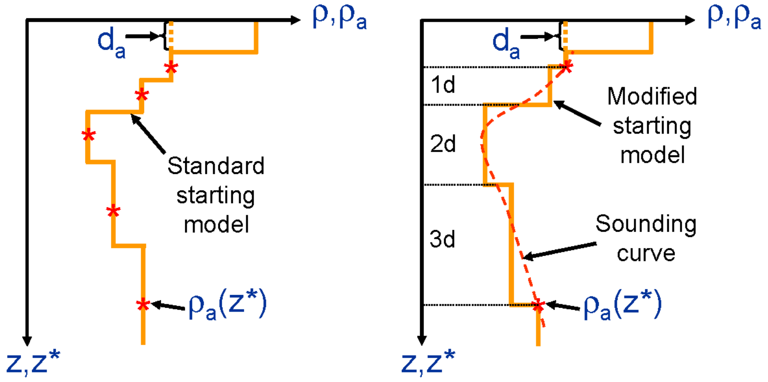

Fig. 5: *Construction of starting models derived from apparent resistivity ρ_a, centroid depth z*, and apparent depth d_a of a five-frequency HEM data set*

The standard model (Siemon, 2006) contains as many layers as frequencies. The layer resistivities are set equal to the apparent resistivities, the layer boundaries are chosen as the logarithmic mean of each two neighbouring centroid depth values. The standard starting model is constructed with respect to the number of frequencies used, i. e., the number of layers is given and the model layers correspond to the apparent resistivities and centroid depths of each frequency. The use of this kind of stating model enables the highest resolution, but also the highest sensitivity to calibration errors. Therefore, a modified starting model is constructed having an arbitrary number of layers. The resistivities and depths of the first and last layers are derived from the apparent resistivities and centroid depths of the highest and lowest frequencies, respectively. These confining layer boundaries can be shifted upwards or downwards. The thicknesses of the intermediate layers increase linearly and the resistivities are picked from an apparent resistivity sounding curve at the corresponding layer centres (on a log scale). Optionally, a resistive cover layer may be used. The thickness of the cover layer is derived from the apparent depth d_a of the highest frequency. If this apparent depth value is less than a minimum layer thickness value, this value (e. g. 0.5 m) is used.

As the laser altitude measurement are affected by the attitude of the HEM system resulting in measured bird altitudes that may be too high, the inversion may derive cover layers being to conductive. To overcome this difficulty, the bird altitude has to be variable. For this, a non-conducting cover layer is introduced representing a variable portion of the bird altitude. During the inversion the thickness of this layer (starting value: 5 m) is optimised.

The inversion procedure is stopped when a given threshold is reached. This threshold is defined as the differential fit of the modelled data to the measured HEM data. Normally a 10% threshold is used; i. e., the inversion stops when the enhancement of the fit is less than 10%.

The data of 5.5 kHz frequency were not used for inversion as they are obtained with a vertical coaxial coil system being sensitive to steeply dipping conductors (and also to external sources) whereas all others are obtained with horizontal coplanar systems.

The survey data were inverted with both types of starting models having five-layers and a highly resistive cover layer. A comparison with borehole data showed that the use of the modified starting model provided the best results.

5.3.8. Presentation of the Results

The HEM results are presented on maps and vertical resistivity sections (VRS). The maps are produced for the half-space parameters, apparent resistivity and centroid depth. Resistivities at ten depth levels (1-120 m below surface) are picked from 1-D inversion models and mapped. All the maps prepared from the results of this survey are listed in **Section 6.3**.

All data points used for the production of apparent resistivity and centroid depth maps are drawn as small black dots (flight lines). White dots mark areas of interpolated data. On the maps displaying resistivities at certain depths, the white dots inform about the number of interpolated data sets: the bigger the dot the more interpolated data were used for the inversion.

The VRS, also based on the 1-D inversion results, are produced for each of the survey lines. These vertical sections are constructed by placing the resistivity models for each sounding point along a survey profile next to each other using the topographic relief as base line (in m asl). The thickness of the bottom layer (substratum) is derived from the corresponding resistivity, but the minimum thickness is 10 m. The altitude of the EM sensor, information about the data processing, the fitting error of the inversion, and the HEM data, which are described in a legend, are plotted above the resistivity models.

5.4. Processing of Magnetic Data

5.4.1. Magnetic Total Field

The earth's total magnetic field T at a point r and at a time t, e. g., measured with an airborne system, is the sum of the following parts:

$$T(r,t) = F(r) + \Delta V(t) + \Delta T(r) + \delta_T(r,t),$$

where

$F(r)$	=	geomagnetic main field (IGRF = International Geomagnetic Reference Field),
$\Delta V(t)$	=	diurnal variations of the earth's magnetic field,
$\Delta T(r)$	=	the crustal field in the survey area,
$\delta_T(r,t)$	=	anthropogenic part of the magnetic field.

The anomalies of the crustal field $\Delta T(r)$, caused by rock magnetization, are of interest. While the IGRF $F(r)$, which can be calculated from table values, and the diurnal variations $\Delta V(t)$, which are recorded at the base station, can be subtracted from the measured total field, the anthropogenic part $\delta_T(r,t)$ cannot be quantified independently. Therefore, the derived ΔT values contain both the geogenic part and the disturbing anthropogenic part. Anthropogenic sources are located at the earth's surface (e. g., buildings, power lines, industrial sites). They are mostly locally constrained and thus can be identified using maps and other sources of information.

5.4.2. IGRF

The IGRF (International Geomagnetic Reference Field) can be calculated for any point on and above the earth's surface at a specific time on the basis of spherical harmonic coefficients, which are updated every five years by the International Association of Geomagnetism and Aeronomy (IAGA, 1992). The geomagnetic main field values of the survey area were calculated for each point using the IGRF-10 model from 2005 (IAGA, 2005).

5.4.3. Diurnal Variations

The base station for recording the time variant parts of the total magnetic field, the diurnal variations, was placed on the airport at 55°13'39"N, 9°16'46"E and 43 m asl. $\Delta V(t)$ values are calculated as the measured value minus the IGRF value for the respective time and place. Possible disturbances of the base station recordings are eliminated using despiking and low-pass (filter width: 20) filters.

5.4.4. Levelling

After subtraction of the main field and diurnal variations from the measured magnetic field values, a statistical levelling is performed. The differences at the intersections of the flight lines and the tie lines are determined and averaged for each flight. The averaged values are then used to correct level errors that may occur in case of changes in the setup of the airborne or base station magnetic sensors during the survey.

Remaining, mostly small level errors may occur, inter alia, as result of different flight directions (heading errors) and are eliminated in a subsequent micro-levelling process. Micro-levelling is based on gridded line data in which level errors are identified using two-dimensional Butterworth high-pass (cut-off value: 500 m, degree: 4) and directional Cosine FFT (azimuth: 90°, degree: 1) filters. Result of the filtering process is an error grid which is sampled along the flight lines. The sampled error values are heavily smoothed using a B-Spline filter (smoothness: 1.05, tension: 0.5) and then subtracted from the original data. Gridding of the levelled data yields a ΔT grid that is virtually free of level errors. Finally, the tie-line data are fit to the levelled line-data grid by removing possible off-sets and trends in their differences.

In (partly) populated areas, grids of ΔT values are mostly dominated by high-amplitude anthropogenic anomalies. These anomalies act as a source of disturbance during the micro-levelling process as well as during the identification of weak geogenic magnetic anomalies. Therefore, a semi-automatic filter procedure is applied to the data prior to micro-levelling. The procedure detects anomalous data in the ΔT grid. Anomalies are detected when the differences of the grid values and their corresponding median values, which are calculated in circular areas shifted over the grid, exceed a given threshold. Manual interaction in the detection process is possible. The resulting grid is, as far as possible, freed from anthropogenic anomalies and is used as input for the micro-levelling process. The anthropogenic regions blanked in the finally levelled data may be re-introduced by applying error values interpolated from neighbouring data sections to them.

The levelled data are used to produce two final ΔT grids. One grid (ΔT) is based on all data including anthropogenic anomalies. A second grid (ΔT_f) is based on the data freed from anthropogenic anomalies, and, additionally, is high-pass filtered. The high-pass filter (cutoff wavelength: 5 km) is applied in order to remove large regional trends in the magnetic field that may mask weak and small-scale geogenic magnetic anomalies. The resulting grid is slightly smoothed using a two-dimensional median filter with a radius two grid cells.

5.4.5. Presentation of the Results

The maps produced to display the magnetic anomaly data are listed in **Section 6.3**. All data points used for map production are drawn as small black dots (flight lines). White dots mark areas of interpolated data.

5.5. Processing of Gamma-Ray Spectrometry Data

The natural gamma radiation of rocks and soil is mainly generated by the radioelements potassium, uranium, and thorium. According to the recommendations of the IAEA (2003), the spectrometry data recorded in the aircraft have to be converted to equivalent ground concentrations of these elements. This requires some preparatory procedures regarding spectrometer calibration and a number of data processing steps listed below.

Spectrometer calibration:

- Determination of cosmic and aircraft background count rates by means of flights over extensive water bodies
- Determination of stripping ratios for Compton scattering correction using calibration pads
- Determination of height attenuation and sensitivity coefficients by means of flights over a calibration range
- Determination of vegetation attenuation coefficients

Data processing:

- Energy calibration
- Reduction of count rate statistical noise
- Determination of detector height above ground and effective height
- Live time correction
- Background correction
- Compton (stripping) correction
- Height-attenuation reduction
- Calculation of equivalent ground concentrations

5.5.1. Energy Calibration

The spectral stability of gamma spectrometers is not perfect. Due to temperature effects, the mapping of energy peaks to correct channel positions may drift slightly during a survey flight. Therefore, an energy calibration is applied to the recorded spectra during data post processing. The channel-energy mapping of a spectrometer can be expressed as follows:

$$ch = E / G + offs,$$

where

ch = channel number,
E = energy in keV,
G = gain constant of spectrometer in keV/channel,
offs = channel offset.

A 256-channel spectrometer has a nominal gain constant of 12.0 keV/channel and an offset of 0 channels. In order to determine the actual gain and offset of the spectrometer used, mean spectra are calculated for each flight line. The positions of the known energy peaks in the mean spectra (K, U, Th) can then be used to calculate actual gain and offset of the instrument during each of the analysed time windows (flight lines). Based on these values, the recorded spectra are re-mapped to a nominal 12 keV/channel raster.

5.5.2. Reduction of Statistical Noise

Due to a relatively large distance between the sources of radiation at the earth's surface and the radiation detector in the helicopter, count rates in airborne gamma-ray surveys are generally low. This results in a high portion of statistical noise present in the recorded spectra and, consequentially, also present in the calculated ground concentrations of radioelements. Therefore, a method for noise reduction developed by Hovgaard & Grasty (1997) is applied to the data. The NASVD method (noise adjusted singular value decomposition) is based on a statistical analysis of all spectra recorded in a survey area and a reconstruction of noise reduced spectra using singular value decomposition routines. The procedure results in smoothed spectra reconstructed from five principal components, from which the count rates for the energy windows of interest (see **Table 6**) are determined. Furthermore, an adaptive filter (Mathis, 1987) for smoothing the count rate channels (filter width: 10) is applied.

5.5.3. Detector Height above Ground and Effective Height

Knowledge of the distance between the source of radiation (on the ground) and the detector (in the helicopter) is crucial for inferring ground concentrations of radioelements from airborne radiometric data correctly. The helicopter system used by BGR is equipped with two altimeters: a radar altimeter in the helicopter and a laser altimeter in the EM bird. Generally, the radar altimeter data are used to determine the detector's height above ground because it is installed on the same platform. However, the data from the laser altimeter are more precise and also contain information on the presence and eventually the thickness of vegetation on the ground beneath the system. Whereas, in forested areas, the radar altimeter detects the tree canopy and underestimates the ground distance, laser altimeter data allow both for estimation of the true ground distance and the vegetation height, which is required for an application of a vegetation attenuation correction (see **Section 5.5.8**). Therefore, a fusion of data from the radar and laser altimeters is performed, resulting in a more accurate estimation of the detector height above ground and an estimation of vegetation height.

In order to apply the radiometric analysis techniques, it is necessary to convert actual environmental conditions of the survey to standard conditions. This includes the adjustment of the measured ground clearance to standard temperature and pressure (STP conditions). The adjusted ground clearance value called "effective height" has the same mass of STP air between the ground and the helicopter as the actual one during data acquisition. The adjustment is applied according to IAEA (2003):

$$h_e = (h_r \cdot P \cdot T_0) / (P_0 \cdot (T + T_0)),$$

where

- h_e = effective height above ground level at STP [m],
- h_r = helicopter height above ground, determined from corrected radar altimeter data [m],
- T_0 = 273.15 K; freezing point of water on Kelvin scale,
- T = air temperature [°C],
- P_0 = 101.325 kPa; mean air pressure at sea level,
- P = barometric pressure [kPa].

5.5.4. Live Time Correction

Gamma-ray spectrometers need a certain amount of time to process a pulse detected by the system. During that time, further incoming pulses are rejected. The amount of time the system is able to detect pulses ("live time") is recorded by the system. Due to the statistical nature of gamma radiation a correction of measured count rates in order to obtain count rate values for a nominal 1 s integration interval (IAEA, 2003) is easily achieved by using the following formula:

$$N = n \cdot 10^3 / t_l,$$

with

- N = corrected count rate,
- n = raw count rate,
- t_l = system live time in milliseconds.

5.5.5. Background Radiation Correction

Cosmic radiation background is caused by high-energy (>3 MeV) cosmic ray particle interaction with the atmosphere. Another source of background radiation is the immanent radioactivity of the helicopter and its equipment. Background radiation distorts the measurements of geogenic radiation and has to be corrected for. The required correction coefficients are determined by means of flights over extensive water bodies at altitudes between 100 and 3500 m. The background correction is applied according to the following formula:

$$N = a + b \cdot C,$$

where

- N = combined cosmic and aircraft background for each channel,
- a = aircraft background for each channel,
- b = cosmic rate stripping factor for each channel,
- C = low-pass filtered cosmic channel (> 3 MeV) count.

The values a and b were determined using data from test flights at different altitudes over the North Sea in 2008. For each channel K, U, Th, and TC (total count) a linear regression of the count rates for different altitude intervals and the filtered cosmic channel count rates revealed values for a and b. The values are listed in **Table 18**.

Table 18: *Aircraft background and cosmic stripping factors*

Channel	Aircraft background a [cps]	Cosmic stripping factor b
TC	31.09	0.722
K	5.51	0.041
U	0.48	0.033
Th	0.33	0.041

5.5.6. Compton Correction

Compton scattering leads to certain amounts of radiation from one energy window being scattered into other energy windows. For example, some amount of thorium radiation will be scattered into lower energy windows such as uranium and potassium. The removal of these effects (Compton correction) is done using so-called stripping ratios. These coefficients describe the magnitudes of scatter between the energy windows of interest. They were determined in 2008 using portable calibration pads (Grasty et al., 1991) and are listed in **Table 19**.

Table 19: *Stripping ratios*

	Stripping ratio	Value
Th → U	α	0.2485
Th → K	β	0.3852
U → K	γ	0.6599
U → Th	a	0.0395

The values of α, β, γ increase with altitude of the helicopter above ground level and have to be corrected on the base of STP equivalent altitude according to the following factors (see IAEA, 2003):

$$\alpha_e = \alpha + 0.00049 \cdot h_e$$
$$\beta_e = \beta + 0.00065 \cdot h_e$$
$$\gamma_e = \gamma + 0.00069 \cdot h_e$$

with

h_e = equivalent height above ground level at STP in metres.

To obtain the net count rates of the particular energy windows, the stripping ratios are applied to the data:

$$N_{Th(corr)} = (N_{Th} - aN_U) / (1 - a\alpha)$$
$$N_{U(corr)} = (N_U - \alpha N_{Th}) / (1 - a\alpha)$$
$$N_{K(corr)} = N_K - \beta N_{Th(corr)} - \gamma N_{U(corr)}$$

where N_{Th}, N_K, N_U represent the background and STP corrected count rates, $N_{Th(corr)}$, $N_{U(corr)}$, $N_{K(corr)}$ are the stripping corrected count rates, and α, β, γ, a are the STP corrected stripping ratios. No Compton correction is applied to the total radiation values (see IAEA, 2003).

5.5.7. Height-Attenuation Reduction

The intensity of gamma radiation measured in airborne surveys varies approximately exponentially with height. In order to estimate count rates at a nominal survey height of 80 m, the following formula is used:

$$N_s = N_m \cdot e^{-\mu (h_0 - h_e)},$$

where

μ = window attenuation coefficient (per metre),
N_m = observed count rate at STP effective height h_e,
N_s = corrected count rate for the nominal survey height h_0.

The values (**Table 20**) were determined from data acquired at different heights over the Allentsteig (Austria) calibration range in 2003.

Table 20: *Height attenuation coefficients*

Window	Height attenuation coefficient μ (per metre at STP)
K	0.007733
U	0.008132
Th	0.005784
TC	0.006468

5.5.8. Radioelement Concentrations and Exposure Rate

IAEA (2003) recommends converting the count rates for the three radioelements into surface concentrations and exposure rates at ground level. The advantage is that the results of measurements with different instruments (e. g. with different crystal volumes) can be compared with each other. Conversion between count rates and concentrations is done using sensitivity coefficients (**Tab. 21**):

$$C = N_s / S,$$

with

C = element concentration (K in %, eU in ppm, eTh in ppm),
N_s = count rate for each window (after height attenuation and stripping),
S = broad source sensitivity for the spectral window.

The calculated concentrations are expressed as equivalent concentrations eU and eTh (in ppm) and as concentrations of K (in %).

Table 21: *Sensitivity coefficients*

Sensitivity
1 % K = 28.42 cps
1 ppm eTh = 1.96 cps
1 ppm eU = 2.92 cps

The sensitivities (**Table 21**) were determined over the Allentsteig (Austria) calibration range. Concentrations calculated this way refer to an infinitely extended and permanently radiating plane. They may differ from the actual concentrations of the elements at ground surface, especially in areas of irregularly distributed radiation sources and under wet conditions. Furthermore, the presence of atmospheric radon may vary considerably during a survey. Radon can spoil radiometric data, in particular uranium concentrations inferred from count rates, because its radiation is detected in the uranium energy window. Presently, there is no correction of the effect of radon radiation on airborne gamma-ray measurements implemented in our radiometric data processing routines. Absolute values of uranium concentrations indicated in the maps are therefore to be regarded with caution.

The calculated concentrations will also be erroneous in areas where vegetation, mostly in the form of trees in forested areas, absorbs part of the radiation from the ground. A vegetation correction can be applied to the data assuming that the attenuation of gamma radiation varies exponentially with vegetation thickness and vegetation thicknesses are known:

$$C_H = C_0 \cdot e^{-\mu \cdot H},$$

where

C_0 = element concentration at the ground,
C_H = element concentration determined in the presence of vegetation,
H = thickness of vegetation,
μ = linear attenuation coefficient of vegetation.

Values for μ (**Table 22**) were determined empirically using extensive data sets acquired over northern Germany. Vegetation thicknesses were inferred from laser altimeter data. In addition to the three radioelements, an attenuation coefficient for the total counts energy window was determined empirically.

Table 22: *Linear attenuation coefficients μ for vegetation.*

Element	μ
K	0.012
U	0.008
Th	0.011
TC	0.006

The ground level exposure rate is calculated as a function of the K, U, and Th concentrations after application of the vegetation correction:

$$E = 1.505 \cdot K + 0.653 \cdot eU + 0.287 \cdot eTh,$$

with

E = ground level exposure rate [μR/h]

using the following conversions (IAEA, 2003):

1 % K = 1.505 μR/h,
1 ppm eU = 0.653 μR/h,
1 ppm eTh = 0.287 μR/h.

5.5.9. Data Levelling and Smoothing

Prior to the vegetation correction and the determination of exposure rates, a statistical levelling of the concentration and total count data is performed. The differences at the intersections of the flight lines and the tie lines are determined and averaged for each flight. The averaged values are then used to correct level errors that may occur in case of environmental changes (e. g. humidity, radon abundance) during the survey.

Remaining, mostly small level errors are eliminated in a subsequent micro-levelling process based on gridded line data in which level errors are identified using two-dimensional Butterworth high-pass (cut-off value: 300 m, degree: 8) and directional Cosine FFT (azimuth: 90°, degree: 1) filters. Result of the filtering process is an error grid which is sampled along the flight lines. The sampled error values are heavily smoothed using a B-Spline filter (smoothness: 0.65 / 0.5, tension: 0.5 / 0.5 for lines / tie lines) and then subtracted from the original data. Gridding of the levelled data yields grids that are virtually free of level errors. Finally, the tie-line data are fit to the levelled line data-grid. This is done by calculating the difference (error) between the values of the levelled line-data grid and the tie-line data, spline smoothing the error and subtracting it from the tie-line data.

Grids of the finally levelled data are slightly smoothed using a two-dimensional median filter of radius 1 (for potassium, thorium and total count) or 2 (for uranium) grid cells. The filtered grids are sampled along the flight path and the sampled data are used as input for vegetation attenuation correction and exposure rate calculations (see previous chapter).

5.5.10. Presentation of the Results

The results of the gamma-ray survey are presented as maps of the equivalent concentrations of the radioelements potassium, uranium, and thorium, total counts, and the ground level exposure rate. The maps produced to display the radiometric data are listed in **Section 6.3**. All data points used for map production are drawn as small black dots (flight lines). White dots mark areas of interpolated data.

Due to technical problems during one flight (13402) no data on the southernmost E–W lines (50.1–68.1) were available and, thus, the final grids differ from the grids of the other methods.

6. Cartographic Work

6.1. Topographic Map

A topographic map was produced as the base map for all thematic maps displaying the airborne geophysical results. A scale of 1:25,000 was chosen for the survey area. An UTM coordinate grid, based on the WGS 84 ellipsoid, is included on the topographic maps. **Table 23** contains the corner coordinates of the map sheet.

Table 23: *Coordinates of the corners of the 1:25,000 Vojens topographic map sheet*

Map corners	Geographic coordinates (WGS 84)		UTM WGS 84 coordinates (Zone 32N)	
	Easting	Northing	Easting	Northing
SW	9°09’26”	55°13’03	510000	6119000
NW	9°09’27”	55°18’26”	510000	6129000
NE	9°21’44”	55°18’25”	523000	6129000
SE	9°21’41”	55°13’01”	523000	6119000

The map is based on the »Topographic Map of Denmark 1:25,000«, © Kort & Matrikelstyrelsen, København. The following map sheets were used:

1212 IV NØ, 1212 IV NV, 1212 IV SØ, 1212 IV SV.

The map has a digitally constructed border and tick marks indicating coordinates in the WGS 84 coordinate system. The grey-shading of the topography of the thematic map has a screen density of 50% of the original digital topographic map.

6.2. Map Production with GEOSOFT and GIS Software

The grids for the geophysical thematic maps were produced using the software package GEOSOFT OASIS montaj 7.2. **Table 24** shows the grid parameters used for the Vojens survey.

Table 24: *Grid parameters*

Parameter	Value
Gridding method	Minimum curvature
Grid size [m]	20
Search radius [m]	20
Internal tension (0-1)	0
Cell extend beyond data	5
Log option	log ρ (else linear)

The final maps including geophysical, topographical and legend information are prepared using the program ESRI ArcGIS 9.3.1. A special plug-in provided by GEOSOFT for ArcGIS (available on DVD or http://www.geosoft.com/resources/releasenotes/plugins/arcGISplugin.asp) is necessary to import and display the GEOSOFT grids as a layer in ArcMap. Adobe Acrobat 9.3 is used for preparing the PDF documents.

6.3. Thematic Maps

Coloured geophysical thematic maps (**Table 25**, **Appendix IV**) were produced at a scale of 1:25,000 for each parameter of interest.

HEM: Apparent resistivities and centroid depths
at 387 Hz, 1,820 Hz, 5,403 Hz, 8,389 Hz, 41,430 Hz, and 133,200 Hz;
Resistivities at 1, 3, 5, 10, 20, 30 ,50, 70 ,90 and 120 m below ground level (bgl);

HMG: Anomalies of the total magnetic field;
Anomalies of the total magnetic field, high-pass filtered, anthropogenic anomalies removed;

HRD: Equivalent concentrations of the radioelements potassium, uranium, and thorium,
total count and ground level exposure rate.

The digital topographic map was used as base map. The surveyed flight lines are plotted in black/white containing information about the quality of the data. In addition, flight-line and elevations maps were produced.

The flight-line maps show the position of the surveyed profiles on the topographic maps. The corresponding line number is shown at the end of a profile at which the flight for that profile commenced. Positions of selected time marks (records), e. g., every 100th, are marked with an “×”. Every tenth plotted time mark is labelled with its number. The flight-line maps permit fast and easy correlation of data from profiles and vertical sections and their position in the survey area.

Digital elevation models (DEM) are derived from the corrected and levelled difference of bird elevation laser altitude. The elevation map also contains the topographic base map and the flight lines.

7. Archiving

All data sets and plots are stored on DVD and archived at BGR section B 2.1 –Geophysical Exploration – Resources and Near Surface Processes. The data formats of processed data are described in **Appendix II**. A technical report, the vertical sections, and the thematic maps (as PDF files) are stored together with the final data (ASCII-coded in GEOSOFT-XYZ format) on a DVD (**Table 25**). A copy of this DVD is attached to this report. The content is listed in **Appendix III**. **Appendix IV** and **Appendix V** contain copies of all maps and vertical resistivity sections, respectively, reduced to smaller scales fitting the A4 format of this report.

Table 25: *Content of the DVD*

Directory		Description of content
\Adobe Acrobat		Adobe® Acrobat Reader in diverse versions for popular system software
\Report		Technical report of the project in PDF format
\Data…	**\HEM**	ASCII file with all raw data (HEM134_RAW.xyz) ASCII file with all processed data (HEM134_DAT.xyz) ASCII file with all derived parameters (HEM134_APP.xyz) ASCII file with results of the 1-D inversion (HEM134_INV.xyz)
\Data…	**\MAG**	ASCII file with data of the total magnetic field, IGRF, base station data, diurnal variations etc. (HMG134.xyz)
\Data…	**\SCI**	ASCII file with data of the equivalent concentrations of potassium, uranium and thorium and the total radiation (HRD134.xyz)
\Maps…	**\HEM**	Apparent resistivity maps and centroid depth maps at a scale of 1:25,000 for the frequencies 387 Hz, 1,820 Hz, 5,403 Hz, 8,389 Hz, 41,430 Hz, 133,200 Hz in PDF format Resistivity maps at a scale of 1:25,000 at 1, 3, 5, 7, 10, 20, 30, 50, 70, 90 and 120 m below surface based on five-layer inversion results in PDF format
\Maps…	**\HMG**	Magnetic anomalies maps at a scale of 1:25,000 in PDF format
\Maps…	**\HRD**	Maps of the equivalent concentrations of the radioelements potassium, uranium, and thorium, the total radiation and the ground level exposure rate at a scale of 1:25,000 in PDF format
\Maps…	**\Flight lines**	Flight line map with topography at a scale of 1:25,000 in PDF format
\Maps…	**\DEM**	Digital elevation model at a scale of 1:25,000 in PDF format
\Maps…	**\ArcGIS**	Map projects for ArcGIS 9.3.1 (*mxd) incl. legends (*bmp), Raster data TK 50 (GRID) and Geosoft-Plugin for ArcGIS
\Vertical sections		Vertical resistivity section based on five-layer inversion results for each profile of the survey area at a horizontal scale of 1:25,000 and at a vertical scale of 1:2,500 in PDF format

8. References

Anderson, W.L., 1989. A hybrid fast Hankel transform algorithm for electromagnetic modelling. Geophysics 54, 263–266.

Grasty, R.L., Holman, P.B. & Blanchard, Y.B., 1991. Transportable calibration pads for ground and airborne gamma-ray spectrometers. Geological survey of Canada, Paper 90-23, 25p.

Hovgaard, J., & Grasty, R.L., 1997. Reducing statistical noise in airborne gamma ray data through spectral component analysis. In "Proceedings of Exploration 97: Fourth Decennial Conference on Mineral Exploration" edited by A.G. Gubins, 753–764.

IAEA, 2003. Guidelines for radioelement mapping using gamma ray spectrometry data. International Atomic Energy Agency. IAEA-TECDOC-1363AEA, Vienna.

Mathis, G.L., 1987. Smoothing spectral gamma logs: A simple but effective technique. Geophysics, 52, 363–367.

IAGA, 1992. International Geomagnetic Reference Field, 1991 Revision. International Association of Geomagnetism and Aeronomy (IAGA) Division V, Working Group 8: Analysis of the main field and secular variation. Geophys. J. Int., 108, 945–946.

IAGA, 2005. International Geomagnetic Reference Field, 2005, 10th generation. International Association of Geomagnetism and Aeronomy, Division V, Working Group V-MOD. http://www.ngdc.noaa.gov/IAGA/vmod/igrf.html.

Johansen, H.K. and Sørensen, K., 1979. The fast Hankel transform. Geophysical Prospecting 27, 876–901.

Naudy, H. & Dreyer, H., 1968. Non-Linear Filtering Applied to Aeromagnetic Profiles. Geophysical Prospecting, 16, 171–178.

Sengpiel, K.-P. & Siemon, B., 2000. Advanced inversion methods for airborne electromagnetic exploration. Geophysics, 65, 1983–1992.

Siemon, B., 2001. Improved and new resistivity-depth profiles for helicopter electromagnetic data. J. Appl. Geophys., 46, 65–76.

Siemon, B., 2006. Electromagnetic methods – frequency domain: Airborne techniques. In: Kirsch, R. (ed.), Groundwater Geophysics – A Tool for Hydrogeology, Springer-Verlag, Berlin, Heidelberg, 155-170.

Siemon, B., 2009. Levelling of frequency-domain helicopter-borne electromagnetic data. Journal of Applied Geophysics, 67, 206–218.

Ward, S.H. & Hohmann, G.W., 1988. Electromagnetic theory for geophysical applications. In Nabighian M.N. (Eds.) Electromagnetic methods in applied geophysics Vol. 1, Theory. Society of Exploration Geophysics, IG no 3, Tulsa, 130–310.

Weidelt, P., 1991, Introduction into electromagnetic sounding. Lecture manuscript. Technical University of Braunschweig, Germany.

BUNDESANSTALT FÜR GEOWISSENSCHAFTEN UND ROHSTOFFE

BGR, HANOVER

(Dr. M. Kosinowski)

Head of Department
„Groundwater and
Soil Science“

(Dr. U. Meyer)

Head of Sub-Department
„Geophysical Exploration –
Resources and
Near Surface Processes“

(Dr. B. Siemon)

Head of Unit
„Airborne Geophysics“

Appendix I

Survey Area 134 – Vojens

Airport:	Vojens, Elevation: 140 ft / 43 m			
Survey parameters:				
Line separation:	Lines:	80 m	Tie lines:	500 m
Line direction:	Lines:	90°	Tie lines:	0°
Line kilometre:	Lines:	596 km	Tie lines:	91 km
Size of area:	54 km²			
Coordinate system:	WGS 84		UTM Zone 32N	
Location of base station:	X: 517475 (9°16'46"E		Y: 6119645 55°13'39"N)	

Table A-1: *Flight table*

Flight	Date	Time (UTC) Start – End	Lines	Remarks
13401	23.06.09	07:58 – 10:18	1.1 W 4.1 E 7.1 W 10.1 E 13.1 W 16.1 E 19.1 W 22.1 E 25.1 W 28.1 E 31.1 W 34.1 E 37.1 W 40.1 E 43.1 W 46.1 E 49.1 W 41.1 E	HELIDAS: SYS14; BKS36a; **EM:** EM4 shortly out after line 49.1 **Magnetometer:** ok **Spectrometer:** ok **Video:** **Weather:** sunny, 12°C, no wind **Line-km:** 156

13402	23.06.09	13:39 – 15:28	50.1 E 51.1 W 52.1 E 53.1 W 54.1 E 55.1 W 56.1 E 57.1 W 58.1 E 59.1 W 60.1 E 61.1 W 62.1 E 63.1 W 64.1 E 65.1 W 66.1 E 67.1 W 68.1 E TL (34.2)	HELIDAS: SYS14; BKS36a; **EM:** EM4 shortly out on and after line 57.1 **Magnetometer:** ok **Spectrometer:** recording of spectral data not ok **Video:** **Weather:** sunny, 26°C, no wind **Line-km:** 152
13403	24.06.09	7:33 – 9:53	48.1 E 47.1 W 45.1 E 41.2 W 44.1 E 45.2 W 42.1 E 39.1 W 38.1 E 35.1 W 36.1 E 33.1 W 32.1 E 29.1 W 30.1 E 27.1 W 26.1 E 23.1 W TL (34.3)	HELIDAS: SYS14; BKS36a; **EM:** EM4 shortly out on and after line 23.1 **Magnetometer:** ok **Spectrometer:** ok **Video:** **Weather:** sunny, 15°C, no wind **Line-km:** 136 Line 45.1 flown in opposite direction, repeated (45.2)

13404	24.06.09	12:26 – 13:36	16.9 N 15.9 S 14.9 N 13.9 S 12.9 N 11.9 S 24.1 E 21.1 W 10.9 N	HELIDAS: SYS14; BKS36a; **EM:** EM4 shortly out on tie line 11.9 System failure after line 21.1 at record 34480 (near radar station on airport) **Magnetometer:** ok **Spectrometer:** ok **Video:** **Weather:** sunny, 23°C, no wind **Line-km:** 65
13405	24.06.09	13:37 – 14:55	1.9 S 2.9 N 3.9 S 4.9 N 5.9 S 6.9 N 7.9 S 8.9 N 9.9 S 10.8 N TL (34.5)	HELIDAS: SYS14; BKS36a; **EM:** ok **Magnetometer:** ok **Spectrometer:** ok **Video:** **Weather:** sunny, 23°C, no wind **Line-km:** 70 Continuation of flight 13404
13406	25.06.09	7:46 – 9:52	20.1 E 17.1 W 18.1 E 15.1 W 14.1 E 11.1 W 12.1 E 9.1 W 8.1 E 5.1 W 6.1 E 3.1 W 2.1 E 41.3 W TL (34.6)	HELIDAS: SYS14; BKS36a; **EM:** EM4 shortly out after line 15.1 **Magnetometer:** ok **Spectrometer:** ok **Video:** **Weather:** sunny, 18°C, no wind **Line-km:** 112

Appendix II

Final Data Format Description

A) Electromagnetics

Description of the four ASCII-coded data files containing the final (levelled) data of a helicopter-borne electromagnetic (HEM) survey

General HEADER:

```
/BGR HEADER (SHORT VERSION):
/
/AREANAME
/VOJENS
/AREACODE
/134
/C_MERIDIAN, ZONE, REFERENCE SYSTEM
/  9 32 WGS84
/ELLIPSOID FOR LON AND LAT
/WGS84
/BIRD
/61
/NUMFREQ
/ 6
/FREQUENCY
/    387.00   1820.00   5403.00   8389.00  41430.00 133200.00
/COILGEOMETRY
/      1.00      1.00      4.00      1.00      1.00      1.00
/COILSEPERATION
/      7.94      7.93      9.06      7.93      7.91      7.92
/TOWCABLE
/ 40.00
/DUMMY
/    -999.990
/DECIMATIONVALUE
/ 1
/PRIVTEXT
(up to five lines of comment may be written here)
```

1) Raw data: HEM134_RAW.XYZ

Example:

```
/Unprocessed data
//Flight 13401
//Date 2009/06/23
Random  0
/     X           Y      LON_BIRD_RAW  LAT_BIRD_RAW  RECORD  UTC_TIME  ALTR    ALTL_FP  ZHG_BIRD_RAW  ZHG_HELI_RAW  ALTB    EM1I  EM1Q ... EM6I  EM6Q  EM1_FREQ ... EM6_FREQ  CPPL    CPSP
526896.00 6124500.00 9.423262  55.266234     0.00    75744.00  1609.12 463.61   490.60        537.71        290.07  6.96  0.00  ...  2.21  3.03  41420.00 ...  5400.00  0.0011  0.0035
526899.00 6124501.00 9.423306  55.266245     1.00    75744.10  1608.73 463.61   490.69        537.81        290.07  6.73  -0.07 ...  2.29  3.10  41419.00 ...  5400.00  0.0010  0.0034
526901.00 6124502.00 9.423349  55.266256     2.00    75744.20  1611.10 463.24   490.78        537.91        289.92  6.58  0.01  ...  1.94  3.21  41417.00 ...  5400.00  0.0017  0.0030
```

In this data file all secondary field values are stored in the order of the following description:

Channel	**Unit**	**Remarks**
X	m	UTM easting in m (WGS 84, Zone 32N), these coordinates have a false easting of 500000 metres
Y	m	UTM northing in m (WGS 84, Zone 32N), these coordinates have no false northing
LON	°	geographic longitude, reference system WGS 84
LAT	°	geographic latitude, reference system WGS 84
RECORD		time mark increasing by 1 every 0.1 seconds
UTC_TIME	hhmmss.s	GPS time (UTC)
ALTR	ft	radar altimeter reading (helicopter)
ALTL_FP	m	laser altimeter reading (bird)
ZHG_BIRD_RAW	m	GPS elevation of the bird, reference system WGS 84
ZHG_HELI_RAW	m	GPS elevation of the helicopter, reference system WGS 84
ALTB	ft	barometric elevation of the helicopter
EM1I	ppm	raw value of the inphase component at the frequency f = 41,430 Hz
EM1Q	ppm	raw value of the quadrature component at the frequency f = 41,430 Hz
EM2I	ppm	raw value of the inphase component at the frequency f = 8,389 Hz
EM2Q	ppm	raw value of the quadrature component at the frequency f = 8,389Hz
EM3I	ppm	raw value of the inphase component at the frequency f = 387 Hz
EM3Q	ppm	raw value of the quadrature component at the frequency f = 387 Hz
EM4I	ppm	raw value of the inphase component at the frequency f = 133,200 Hz
EM4Q	ppm	raw value of the quadrature component at the frequency f = 133,200 Hz
EM5I	ppm	raw value of the inphase component at the frequency f = 1,820 Hz
EM5Q	ppm	raw value of the quadrature component at the frequency f = 1,820 Hz
EM6I	ppm	raw value of the inphase component at the frequency f = 5,403 Hz, converted to horizontal coplanar
EM6Q	ppm	raw value of the quadrature component at the frequency f = 5,403 Hz, converted to horizontal coplanar

EM1_FREQ	Hz	frequency of EM1 channels (f = 41,430 Hz)
EM2_FREQ	Hz	frequency of EM2 channels (f = 8,389 Hz)
EM3_FREQ	Hz	frequency of EM3 channels (f = 387 Hz)
EM4_FREQ	Hz	frequency of EM4 channels (f = 133,200 Hz)
EM5_FREQ	Hz	frequency of EM5 channels (f = 1,820 Hz)
EM6_FREQ	Hz	frequency of EM6 channels (f = 5,403 Hz)
CPPL		power-line detector
CPSP		sferics detector

Remarks:
Lines starting with "/" comment,
Lines starting with "//" flight number and date,
Lines starting with "Random" original flights.

Original vertical coaxial data are indicated by -0.25 (instead of 4.00 for converted data):
/COILGEOMETRY
/ 1.00 1.00 -0.25 1.00 1.00 1.00

General Remarks for the next three data sets:
Lines starting with "/" comment,
Lines starting with "//" flight number and date,
Lines starting with "Line" lines,
Lines starting with "Tie" tie lines.

2) Data: HEM134_DAT.XYZ

Example:

```
/Processing by A. Ullmann (BGR) using Oasis montaj
/Levelled data
/    X          Y          LON         LAT       RECORD    UTC     TOPO  H_RADAR  H_LASER BIRD_NN  H_BARO  REAL_1  QUAD_1 ... REAL_6  QUAD_6
//Flight 13401
//Date 2009/06/23
Line  1.1
 521355  6127061  9.336263  55.289514  6640   80848.0  50.42   101.28    97.1    1147.53   145.64   3.390   0.468  ...  4.046   6.518
 521352  6127060  9.336212  55.289513  6641   80848.1  50.32   100.26    96.60    146.92   143.41   3.390   0.468  ...  4.046   6.518
 521349  6127060  9.336161  55.289511  6642   80848.2  50.22    99.78    96.10    146.32   144.16   3.004   1.075  ...  2.898   4.980
```

In this data file all necessary position parameters and secondary field values are stored in the order of the following description:

Channel	Unit	Remarks
X	m	UTM easting in m (WGS 84, Zone 32N), these coordinates have a false easting of 500000 metres
Y	m	UTM northing in m (WGS 84, Zone 32N), these coordinates have no false northing
LON	°	geographic longitude, reference system WGS 84
LAT	°	geographic latitude, reference system WGS 84
RECORD		time mark increasing by 1 every 0.1 seconds
UTC_TIME	hhmmss.s	GPS time (UTC)
TOPO	m	levelled topographic elevation (in metre above sea level), derived from the difference of bird elevation (BIRN_NN) and bird altitude (H_LASER)
H_RADAR	m	smoothed value of the radar altitude minus the effective cable length (40 m) from the helicopter to the bird, corresponds to the bird altitude
H_LASER	m	smoothed value of the laser altimeter, corresponds to the bird
BIRD_NN	m	smoothed bird elevation (in m asl = metre above sea level), reference system: WGS84
H_BARO	m	processed value of the barometric sensor minus the effective cable length (40 m) from the helicopter to the bird
REAL_1	ppm	processed value of the inphase component at the frequency f = 387 Hz
QUAD_1	ppm	processed value of the quadrature component at the frequency f = 387 Hz
REAL_2	ppm	processed value of the inphase component at the frequency f = 1,820 Hz
QUAD_2	ppm	processed value of the quadrature component at the frequency f = 1,820 Hz
REAL_3	ppm	processed value of the inphase component at the frequency f = 5,403 Hz, converted to horizontal coplanar
QUAD_3	ppm	processed value of the quadrature component at the frequency f = 5,403 Hz, converted to horizontal coplanar
REAL_4	ppm	processed value of the inphase component at the frequency f = 8,389 Hz
QUAD_4	ppm	processed value of the quadrature component at the frequency f = 8,389 Hz
REAL_5	ppm	processed value of the inphase component at the frequency f = 41,430 Hz
QUAD_5	ppm	processed value of the quadrature component at the frequency f = 41,430 Hz
REAL_6	ppm	processed value of the inphase component at the frequency f = 133,200 Hz
QUAD_6	ppm	processed value of the quadrature component at the frequency f = 133,200 Hz

3) Half-space parameters: HEM134_APP.XYZ

Example:

```
/Processing by A. Ullmann (BGR) using Oasis montaj
/Levelled data
/    X         Y         LON        LAT       RECORD  UTC     TOPO  H_RADAR H_LASER BIRD_NN  H_BARO  RHOA_1  KDA_1  ZST_1 ... RHOA_6  KDA_6  ZST_6
//Flight 13401
//Date 2009/06/23
Line  1.1
 521355  6127061  9.336263  55.289514   6640  80848.0  50.42   101.28   97.11   147.53   145.64   28.60   11.56   80.06 ...  38.06   -0.01   4.24
 521352  6127060  9.336212  55.289513   6641  80848.1  50.32   100.26   96.60   146.92   143.41   28.51   11.40   79.79 ...  40.19   -0.04   4.33
 521349  6127060  9.336161  55.289511   6642  80848.2  50.22    99.78   96.10   146.32   144.16   28.44   11.24   79.54 ...  42.17   -0.09   4.39
```

In this data file all necessary position parameters and half-space parameters are stored in the order of the following description:

Channel	**Unit**	**Remarks**
X	m	UTM easting in m (WGS 84, Zone 32N), these coordinates have a false easting of 500000 metres
Y	m	UTM northing in m (WGS 84, Zone 32N), these coordinates have no false northing
LON	°	geographic longitude, reference system WGS 84
LAT	°	geographic latitude, reference system WGS 84
RECORD		time mark increasing by 1 every 0.1 seconds
UTC_TIME	hhmmss.s	GPS time (UTC)
TOPO	m	levelled topographic elevation (in metre above sea level), derived from the difference of bird elevation (BIRN_NN) and bird altitude (H_LASER)
H_RADAR	m	smoothed value of the radar altitude minus the effective cable length (40 m) from the helicopter to the bird, corresponds to the bird altitude
H_LASER	m	smoothed value of the laser altimeter, corresponds to the bird
BIRD_NN	m	smoothed bird elevation (in m asl = metre above sea level), reference system: WGS84
H_BARO	m	filtered value of the barometric sensor minus the effective cable length (40 m) from the helicopter to the bird
RHOA_1	Ωm	apparent resistivity at the frequency f = 387 Hz
KDA_1	m	apparent depth at the frequency f = 387 Hz
ZST_1	m	centroid depth at the frequency f = 387 Hz
RHOA_2	Ωm	apparent resistivity at the frequency f = 1,820 Hz
KDA_2	m	apparent depth at the frequency f = 1,820 Hz
ZST_2	m	centroid depth at the frequency f = 1,820 Hz
RHOA_3	Ωm	apparent resistivity at the frequency f = 5,403 Hz
KDA_3	m	apparent depth at the frequency f = 5,403 Hz
ZST_3	m	centroid depth at the frequency f = 5,403 Hz
RHOA_4	Ωm	apparent resistivity at the frequency f = 8,389 Hz
KDA_4	m	apparent depth at the frequency f = 8,389 Hz
ZST_4	m	centroid depth at the frequency f = 8,389 Hz
RHOA_5	Ωm	apparent resistivity at the frequency f = 41,430 Hz
KDA_5	m	apparent depth at the frequency f = 41,430 Hz
ZST_5	m	centroid depth at the frequency f = 41,430 Hz
RHOA_6	Ωm	apparent resistivity at the frequency f = 133,200 Hz
KDA_6	m	apparent depth at the frequency f = 133,200 Hz
ZST_6	m	centroid depth at the frequency f = 133,200 Hz

4) Inversion models HEM134_INV.XYZ

Example

```
/Processing by A. Ullmann (BGR) using Oasis montaj
/Levelled data
/    X         Y         LON        LAT      RECORD   UTC     TOPO  H_RADAR  H_LASER  BIRD_NN  H_BARO  RHO_I_1  D_I_1    ...   RHO_I_4  D_I_4  RHO_I_5  QALL
//Flight 13401
//Date 2009/06/23
Line  1.1
 521355  6127061  9.336263  55.289514  6640  80848.0  50.42  101.28  97.11  147.53  145.64  37.53  4.41  ...  43.83  62.36  27.81  5.19
 521352  6127060  9.336212  55.289513  6641  80848.1  50.32  100.26  96.60  146.92  143.41  41.36  5.29  ...  40.33  59.25  30.09  5.28
 521349  6127060  9.336161  55.289511  6642  80848.2  50.22   99.78  96.10  146.32  144.16  44.21  6.47  ...  37.54  61.99  31.80  5.32
```

In this data file all necessary position parameters and inversion models are stored in the order of the following description:

Channel	Unit	Remarks
X	m	UTM easting in m (WGS 84, Zone 32N), these coordinates have a false easting of 500000 metres
Y	m	UTM northing in m (WGS 84, Zone 32N), these coordinates have no false northing
LON	°	geographic longitude, reference system WGS 84
LAT	°	geographic latitude, reference system WGS 84
RECORD		time mark increasing by 1 every 0.1 seconds
UTC_TIME	hhmmss.s	GPS time (UTC)
TOPO	m	levelled topographic elevation (in metre above sea level), derived from the difference of bird elevation (BIRN_NN) and bird altitude (H_LASER)
H_RADAR	m	smoothed value of the radar altitude minus the effective cable length (40 m) from the helicopter to the bird, corresponds to the bird altitude
H_LASER	m	smoothed value of the laser altimeter, corresponds to the bird
BIRD_NN	m	smoothed bird elevation (in m asl = metre above sea level), reference system: WGS84
H_BARO	m	filtered value of the barometric sensor minus the effective cable length (40 m) from the helicopter to the bird
RHO_I_1	Ωm	resistivity of the top layer of a five-layer inversion model
D_I_1	m	thickness of the top layer of a five-layer inversion model
RHO_I_2	Ωm	resistivity of the second layer of a five-layer inversion model
D_I_2	m	thickness of the second layer of a five-layer inversion model
RHO_I_3	Ωm	resistivity of the third layer of a five-layer inversion model
D_I_3	m	thickness of the third layer of a five-layer inversion model
RHO_I_4	Ωm	resistivity of the fourth layer of a five-layer inversion model
D_I_4	m	thickness of the fourth layer of a five-layer inversion model
RHO_I_5	Ωm	resistivity of the fifth layer of a five-layer inversion model
QALL	%	misfit of the inversion (L1 norm)

Remarks:

The header contains following additional lines:

```
/IFREQUENCY
/   1    1    0    1    1    1
/NUMLAYER
/   5
/MUELAYER
/   0
```

B) Magnetics

Description of the ASCII coded data file **HMG134.XYZ** containing the final (levelled) data of a helicopter-borne magnetic (HMG) survey
Example:

```
/   X        Y        LON        LAT       RECORD  UTC_DATE   UTC_TIME  ALT_BIRD  H_RADAR_RAW  H_LASER_RAW  T_BASE_RAW  T_BASE_F  T_RAW  DELTA_T  DELTA_T_LEV  DELTA_T_FILT
//Flight 13401
//Date 2009/06/23
Line  1.1
521355  6127061 9.336263  55.289514  6640   20090623   80848.0   143.3     453.5        96.1    49881.29   49881.28  50058.42  160.60   159.62   -1.33
521352  6127060 9.336212  55.289513  6641   20090623   80848.1   142.7     453.4        96.1    49881.29   49881.28  50058.34  160.58   159.59   -1.32
521349  6127060 9.336161  55.289511  6642   20090623   80848.2   142.1     451.4        95.0    49881.29   49881.28  50058.27  160.55   159.56   -1.31
```

In this data file all necessary position parameters and magnetic data are stored in the order of the following description:

Channel	Unit	Remarks
X	m	UTM easting in m (WGS 84, Zone 32N), these coordinates have a false easting of 500000 metres
Y	m	UTM northing in m (WGS 84, Zone 32N), these coordinates have no false northing
LON	°	geographic longitude, reference system WGS 84
LAT	°	geographic latitude, reference system WGS 84
RECORD		time mark increasing by 1 every 0.1 seconds
UTC_DATE	yyyymmdd	date
UTC_TIME	hhmmss.s	GPS time (UTC)
ALT_BIRD	m	smoothed bird elevation (in m asl = metre above sea level), reference system: WGS84
H_RADAR	m	smoothed value of the radar altitude minus the effective cable length (40 m) from the helicopter to the bird, corresponds to the bird altitude
H_LASER	m	smoothed value of the laser altimeter, corresponds to the bird
T_BASE_RAW	nT	raw data of the magnetic field at the base station
T_BASE_F	nT	processed data of the magnetic field at the base station
T_RAW	nT	raw data of the magnetic field at the bird
DELTA_T	nT	anomalies of the magnetic field
DELTA_T_LEV	nT	levelled anomalies of the magnetic field
DELTA_T_FILT	nT	(high-pass) filtered anomalies of the magnetic field, corrected for man-made effects

Remarks:

Lines starting with "/"	comment,
Lines starting with "//"	flight number and date,
Lines starting with "Line"	lines,
Lines starting with "Tie"	tie lines.

C) Radiometry

Description of the ASCII coded data file **HRD134.XYZ** containing the final (levelled) data of a helicopter-borne radiometric (HRD) survey

Example:

```
/  X       Y         LON       LAT       RECORD    UTC_DATE  UTC_TIME  ALT_BIRD  H_RADAR_RAW  H_LASER_RAW  HAG  PRESSURE  TEMP  LIVE_T  COSMIC_RAW  TOT_RAW  POT_RAW  URA_RAW  THO_RAW  URAUP_RAW
Continuation of last line:
                TOT    POT    URA    THO    TOT_LEV  POT_LEV  URA_LEV  THO_LEV  EXPO
//Flight 13401
//Date 2009/06/23
Line  1.1
521355  6127061 9.336263  55.289514  6640  20090623  80848.0 143.3  453.5  96.1  138.8 101.410  15.9  960  74  387  48  8   12  0
521323  6127059 9.335751  55.289501  6650  20090623  80849.0 137.3  441.1  92.0  134.1 101.478  15.9  938  61  421  53  6   8   1
521290  6127057 9.335238  55.289482  6660  20090623  80850.0 131.3  418.6  87.5  129.3 101.562  15.9  954  72  390  45  11  9   1
Continuation of last three lines:
          473.1  1.94  2.10  5.33  483.08  1.98  2.23  5.49  6.01
          472.1  2.02  2.29  6.19  477.92  2.01  2.22  5.86  6.15
          449.7  1.83  2.01  5.25  459.95  1.90  2.16  5.53  5.85
```

In this data file all necessary position parameters and radiometric data are stored in the order of the following description:

Channel	**Unit**	**Remarks**
X	m	UTM easting in m (WGS 84, Zone 32N), these coordinates have a false easting of 500000 metres
Y	m	UTM northing in m (WGS 84, Zone 32N), these coordinates have no false northing
LON	°	geographic longitude, reference system WGS 84
LAT	°	geographic latitude, reference system WGS 84
RECORD		time mark increasing by 1 every 0.1 seconds
UTC_DATE	yyyymmdd	date
UTC_TIME	hhmmss.s	GPS time (UTC)
ALT_BIRD	m	smoothed bird elevation (in m asl = metre above sea level), reference system: WGS84
H_RADAR_RAW	m	value of the radar altitude minus the effective cable length (40 m) from the helicopter to the bird, corresponds to the bird altitude
H_LASER_RAW	m	value of the laser altimeter, corresponds to the bird
HAG	m	altitude of helicopter above ground level
PRESSURE	kPa	air pressure
TEMP	°C	air temperature
LIVE_T	ms	live time
COSMIC	cps	cosmic radiation > 3 MeV
TOT_RAW	cps	measured total count rate
POT_RAW	cps	measured potassium count rate
URA_RAW	cps	measured uranium count rate
THO_RAW	cps	measured thorium count rate
URAUP	cps	measured uranium count rate in upward looking crystal

TOT	cps	total count
POT	%	potassium concentration on ground level
URA	ppm	equivalent uranium concentration ground level
THO	ppm	equivalent thorium concentration ground level
TOT_LEV	cps	levelled total count, corrected for the effect of vegetation
POT_LEV	%	levelled potassium concentration on ground level, corrected for the effect of vegetation
URA_LEV	ppm	levelled equivalent uranium concentration on ground level, corrected for the effect of vegetation
THO_LEV	ppm	levelled equivalent thorium concentration on ground level, corrected for the effect of vegetation
EXPO	µR/h	ground level exposure rate

Remarks:

Lines starting with "/"	comment,
Lines starting with "//"	flight number and date,
Lines starting with "Line"	lines,
Lines starting with "Tie"	tie lines.

Appendix III

DVD

Adobe PDF

\Acrobat Reader
- Adobe - Adobe Reader herunterladen.URL
- \Acrobat Reader\Linux\
- AdbeRdr9.3.4-1_i486linux_deu.bin
- \Acrobat Reader\Mac\
- AdbeRdr930_de_DE_i386.pkg.zip
- \Acrobat Reader\Windows
- AdbeRdr934_de_DE.exe

\Data
- \Data HEM
- Format_description_HEM134.txt
- HEM134_APP.XYZ
- HEM134_DAT.XYZ
- HEM134_INV.xyz
- HEM134_RAW.XYZ

\Data HMG
- Format_description_HMG134.txt
- HMG134.XYZ

\Data HRD
- Format_description_HRD134.txt
- HRD134.XYZ

\Maps
- \Maps\ArcGis
- 134 Vojens apparent resistivity rhoa1.mxd
- 134 Vojens apparent resistivity rhoa2.mxd
- 134 Vojens apparent resistivity rhoa3.mxd
- 134 Vojens apparent resistivity rhoa4.mxd
- 134 Vojens apparent resistivity rhoa5.mxd
- 134 Vojens apparent resistivity rhoa6.mxd
- 134 Vojens centroid depth zst1.mxd
- 134 Vojens centroid depth zst2.mxd
- 134 Vojens centroid depth zst3.mxd
- 134 Vojens centroid depth zst4.mxd
- 134 Vojens centroid depth zst5.mxd
- 134 Vojens centroid depth zst6.mxd
- 134 Vojens DEM.mxd
- 134 Vojens exposure rate.mxd
- 134 Vojens flight lines.mxd
- 134 Vojens magnetic anomalies filtered.mxd
- 134 Vojens magnetic anomalies.mxd
- 134 Vojens Potassium.mxd
- 134 Vojens resistivity -001m.mxd
- 134 Vojens resistivity -003m.mxd
- 134 Vojens resistivity -005m.mxd
- 134 Vojens resistivity -010m.mxd
- 134 Vojens resistivity -020m.mxd
- 134 Vojens resistivity -030m.mxd
- 134 Vojens resistivity -050m.mxd
- 134 Vojens resistivity -070m.mxd
- 134 Vojens resistivity -090m.mxd
- 134 Vojens resistivity -120m.mxd
- 134 Vojens Thorium.mxd
- 134 Vojens total count.mxd
- 134 Vojens Uranium.mxd

\Maps\ArcGis\Legends
- 134 Vojens Legende apparent resistivity rhoa1.bmp
- 134 Vojens Legende apparent resistivity rhoa2.bmp
- 134 Vojens Legende apparent resistivity rhoa3.bmp
- 134 Vojens Legende apparent resistivity rhoa4.bmp
- 134 Vojens Legende apparent resistivity rhoa5.bmp
- 134 Vojens Legende apparent resistivity rhoa6.bmp
- 134 Vojens Legende centroid depth zst1.bmp
- 134 Vojens Legende centroid depth zst2.bmp
- 134 Vojens Legende centroid depth zst3.bmp
- 134 Vojens Legende centroid depth zst4.bmp
- 134 Vojens Legende centroid depth zst5.bmp
- 134 Vojens Legende centroid depth zst6.bmp
- 134 Vojens Legende DEM.bmp
- 134 Vojens Legende Exposure rate.bmp
- 134 Vojens Legende flight lines.bmp
- 134 Vojens Legende magnetic anomalies filtered.bmp
- 134 Vojens Legende magnetic anomalies.bmp
- 134 Vojens Legende Potassium.bmp
- 134 Vojens Legende resistivity -001m.bmp
- 134 Vojens Legende resistivity -003m.bmp
- 134 Vojens Legende resistivity -005m.bmp
- 134 Vojens Legende resistivity -010m.bmp
- 134 Vojens Legende resistivity -020m.bmp
- 134 Vojens Legende resistivity -030m.bmp
- 134 Vojens Legende resistivity -030m.tif
- 134 Vojens Legende resistivity -050m.bmp
- 134 Vojens Legende resistivity -070m.bmp
- 134 Vojens Legende resistivity -090m.bmp
- 134 Vojens Legende resistivity -120m.bmp
- 134 Vojens Legende Thorium.bmp
- 134 Vojens Legende Total count.bmp
- 134 Vojens Legende Uranium.bmp

\Maps\ArcGis\Oasis
- EXPO.grd
- expo.map
- expo.map.xml
- flightlines_P.map
- flightlines_P.map.xml
- hsp_P1.map
- hsp_P1.map.xml
- hsp_P2.map
- hsp_P2.map.xml
- hsp_P3.map
- hsp_P3.map.xml
- hsp_P4.map
- hsp_P4.map.xml
- hsp_P5.map
- hsp_P5.map.xml
- hsp_P6.map
- hsp_P6.map.xml
- mag.map
- mag.map.xml

mag_filt.map
mag_filt.map.xml
mag_filt_P.map
mag_filt_P.map.xml
MAG_LEV.grd
MAG_LEV_CE_BP_M2_S.grd
mag_P.map
mag_P.map.xml
pot.map
pot.map.xml
POT_BIO.grd
rho_001m.grd
rho_001m.map
rho_001m.map.xml
rho_003m.grd
rho_003m.map
rho_003m.map.xml
rho_005m.grd
rho_005m.map
rho_005m.map.xml
rho_010m.grd
rho_010m.map
rho_010m.map.xml
rho_020m.grd
rho_020m.map
rho_020m.map.xml
rho_030m.grd
rho_030m.map
rho_030m.map.xml
rho_050m.grd
rho_050m.map
rho_050m.map.xml
rho_070m.grd
rho_070m.map
rho_070m.map.xml
rho_090m.grd
rho_090m.map
rho_090m.map.xml
rho_090m_P.map
rho_090m_P.map.xml
rho_120m.grd
rho_120m.map
rho_120m.map.xml
rho_120m_P.map
rho_120m_P.map.xml
rho_P.map
rho_P.map.xml
rhoa1.map
rhoa1.map.xml
rhoa1_LEV_IQ.GRD
rhoa2.map
rhoa2.map.xml
rhoa2_LEV_IQ.GRD
rhoa3.map
rhoa3.map.xml
rhoa3_LEV_IQ.GRD
rhoa4.map
rhoa4.map.xml
rhoa4_LEV_IQ.GRD
rhoa5.map
rhoa5.map.xml
rhoa5_LEV_IQ.GRD
rhoa6.map
rhoa6.map.xml
rhoa6_LEV_IQ.GRD
tho.map
tho.map.xml
THO_BIO.grd
tot.map
tot.map.xml
TOT_BIO.grd
ura.map
ura.map.xml
URA_BIO.grd
zst1.map
zst1.map.xml
zst1_LEV_IQ.GRD
zst2.map
zst2.map.xml
zst2_LEV_IQ.GRD
zst3.map
zst3.map.xml
zst3_LEV_IQ.GRD
zst4.map
zst4.map.xml
zst4_LEV_IQ.GRD
zst5.map
zst5.map.xml
zst5_LEV_IQ.GRD
zst6.map
zst6.map.xml
zst6_LEV_IQ.GRD

\Maps\ArcGis\Topography
1212_IV_NØ.tfw
1212_IV_NØ.tif
1212_IV_NV.tfw
1212_IV_NV.tif
1212_IV_SØ.tfw
1212_IV_SØ.tif
1212_IV_SV.tfw
1212_IV_SV.tif
134 Vojens TK Schnitt - Kopie.tfw
134 Vojens TK Schnitt - Kopie.tif
134 Vojens TK Schnitt.tfw
134 Vojens TK Schnitt.tif

\Maps\DEM
134 Vojens DEM.pdf

\Maps\Flightlines
134 Vojens flight lines.pdf

\Maps\HEM
134 Vojens apparent resistivity rhoa1.pdf
134 Vojens apparent resistivity rhoa2.pdf
134 Vojens apparent resistivity rhoa3.pdf
134 Vojens apparent resistivity rhoa4.pdf
134 Vojens apparent resistivity rhoa5.pdf
134 Vojens apparent resistivity rhoa6.pdf
134 Vojens centroid depth zst1.pdf
134 Vojens centroid depth zst2.pdf
134 Vojens centroid depth zst3.pdf
134 Vojens centroid depth zst4.pdf
134 Vojens centroid depth zst5.pdf
134 Vojens centroid depth zst6.pdf
134 Vojens resistivity -001m.pdf
134 Vojens resistivity -003m.pdf

134 Vojens resistivity -005m.pdf
134 Vojens resistivity -010m.pdf
134 Vojens resistivity -020m.pdf
134 Vojens resistivity -030m.pdf
134 Vojens resistivity -050m.pdf
134 Vojens resistivity -070m.pdf
134 Vojens resistivity -090m.pdf
134 Vojens resistivity -120m.pdf

\Maps\HMG
134 Vojens magnetic anomalies filtered.pdf
134 Vojens magnetic anomalies.pdf

\Maps\HRD
134 Vojens exposure rate.pdf
134 Vojens Potassium.pdf
134 Vojens Thorium.pdf
134 Vojens total count.pdf
134 Vojens Uranium.pdf

\Report
Technical Report 134 Vojens.pdf

\VRS
VRS 1340011.PDF
VRS 1340019.PDF
VRS 1340021.PDF
VRS 1340029.PDF
VRS 1340031.PDF
VRS 1340039.PDF
VRS 1340041.PDF
VRS 1340049.PDF
VRS 1340051.PDF
VRS 1340059.PDF
VRS 1340061.PDF
VRS 1340069.PDF
VRS 1340071.PDF
VRS 1340079.PDF
VRS 1340081.PDF
VRS 1340089.PDF
VRS 1340091.PDF
VRS 1340099.PDF
VRS 1340101.PDF
VRS 1340108.PDF
VRS 1340111.PDF
VRS 1340119.PDF
VRS 1340121.PDF
VRS 1340129.PDF
VRS 1340131.PDF
VRS 1340139.PDF
VRS 1340141.PDF
VRS 1340149.PDF
VRS 1340151.PDF
VRS 1340159.PDF
VRS 1340161.PDF
VRS 1340169.PDF
VRS 1340171.PDF
VRS 1340181.PDF
VRS 1340191.PDF
VRS 1340201.PDF
VRS 1340211.PDF
VRS 1340221.PDF
VRS 1340231.PDF
VRS 1340241.PDF
VRS 1340251.PDF
VRS 1340261.PDF
VRS 1340271.PDF
VRS 1340281.PDF
VRS 1340291.PDF
VRS 1340301.PDF
VRS 1340311.PDF
VRS 1340321.PDF
VRS 1340331.PDF
VRS 1340341.PDF
VRS 1340351.PDF
VRS 1340361.PDF
VRS 1340371.PDF
VRS 1340381.PDF
VRS 1340391.PDF
VRS 1340401.PDF
VRS 1340413.PDF
VRS 1340421.PDF
VRS 1340431.PDF
VRS 1340441.PDF
VRS 1340452.PDF
VRS 1340461.PDF
VRS 1340471.PDF
VRS 1340481.PDF
VRS 1340491.PDF
VRS 1340501.PDF
VRS 1340511.PDF
VRS 1340521.PDF
VRS 1340531.PDF
VRS 1340541.PDF
VRS 1340551.PDF
VRS 1340561.PDF
VRS 1340571.PDF
VRS 1340581.PDF
VRS 1340591.PDF
VRS 1340601.PDF
VRS 1340611.PDF
VRS 1340621.PDF
VRS 1340631.PDF
VRS 1340641.PDF
VRS 1340651.PDF
VRS 1340661.PDF
VRS 1340671.PDF
VRS 1340681.PDF

Appendix IV

Maps

(reduced to a scale of 1:75,000)

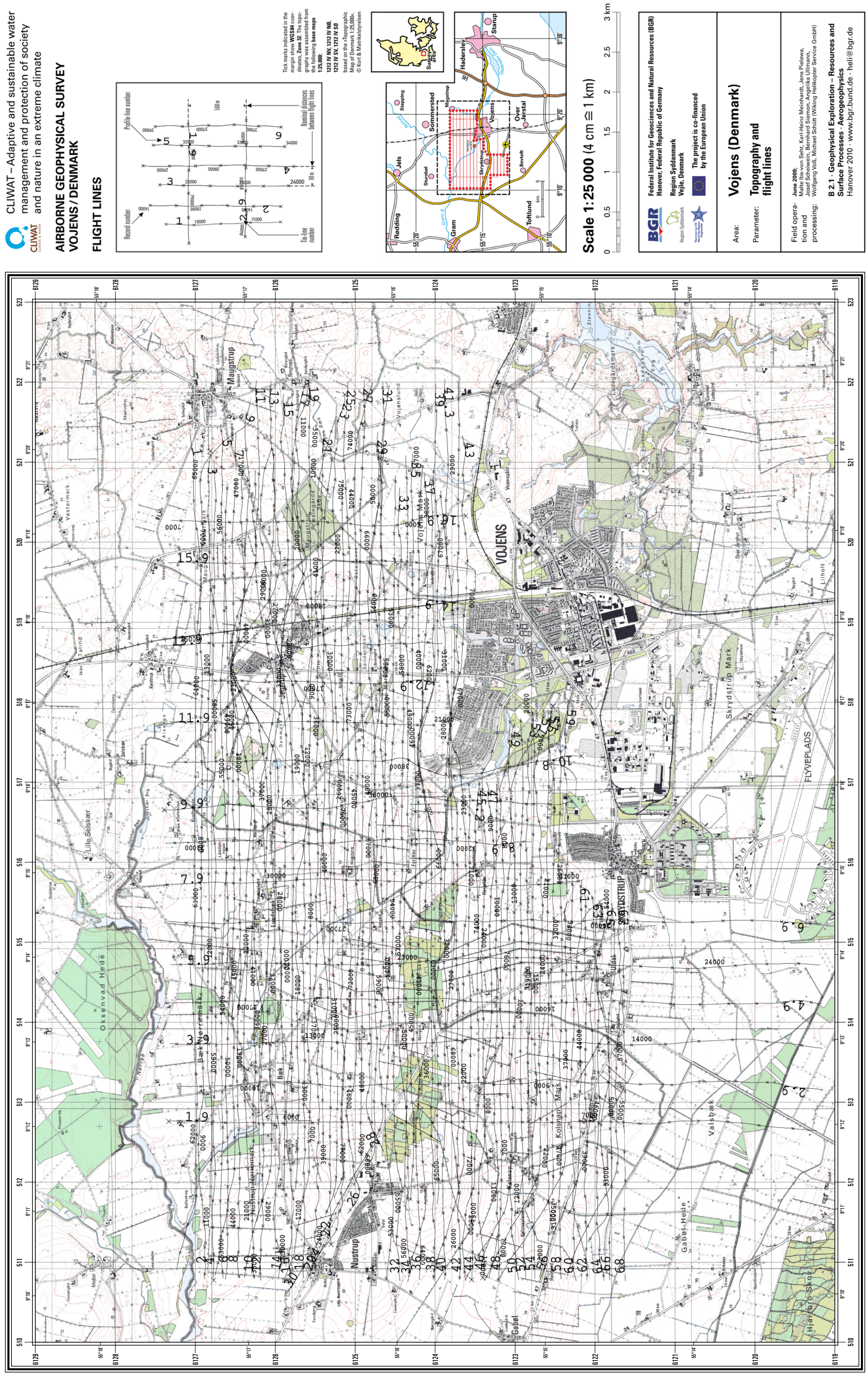
CLIWAT – Adaptive and sustainable water management and protection of society and nature in an extreme climate
AIRBORNE GEOPHYSICAL SURVEY
VOJENS / DENMARK
FLIGHT LINES
Scale 1:25 000 (4 cm ≙ 1 km)
Federal Institute for Geosciences and Natural Resources (BGR) Hanover, Federal Republic of Germany
Region Syddanmark Vejle, Denmark
The project is co-financed by the European Union
Area: Vojens (Denmark)
Parameter: Topography and flight lines
B 2.1 · Geophysical Exploration – Resources and Surface Processes · Aerogeophysics
Hanover 2010 · www.bgr.bund.de · heli@bgr.de
VOJENS
SKRYDSTRUP
FLYVEPLADS
Nustrup

Alle anderen Karten und Vertikal-
sektionen sind in dieser Web-Fassung
des Berichtes nicht enthalten.

All other maps and vertical
resistivity sections are not included
in this web edition of the report.